Coordination Chemistry Reviews 253 (2009) 2998–3014

Contents lists available at ScienceDirect

Coordination Chemistry Reviews

journal homepage: www.elsevier.com/locate/ccr

Review

Amorphous silica nanohybrids: Synthesis, properties and applications

Yuhui Jin, Aize Li, Sandra G. Hazelton, Song Liang, Carrie L. John, Paul D. Selid, David T. Pierce, Julia Xiaojun Zhao*

Department of Chemistry, University of North Dakota, Grand Forks, ND 58203, USA

Contents

1. Introduction 2999
2. Molecule–silica nanohybrids 2999
   2.1. Fluorescent nanohybrids 2999
      2.1.1. Synthesis 2999
      2.1.2. Properties and applications 3001
   2.2. Chemiluminescent nanohybrids 3002
      2.2.1. Chemiluminescence pathways 3002
      2.2.2. Properties and applications 3002
   2.3. Drug transporting nanohybrids 3003
      2.3.1. Synthesis 3003
      2.3.2. Properties and applications 3004
3. Functional nanomaterial-silica nanohybrids 3005
   3.1. Quantum dot nanohybrids 3006
      3.1.1. Synthesis 3006
      3.1.2. Properties and applications 3007
   3.2. Magnetic nanoparticle nanohybrids 3008
      3.2.1. Synthesis 3008
      3.2.2. Properties and applications 3008
   3.3. Gold nanomaterial nanohybrids 3009
      3.3.1. Synthesis 3009
      3.3.2. Properties and applications 3010
   3.4. Catalytic nanohybrids 3011
      3.4.1. Silica-based metal catalysts 3011
      3.4.2. Silica-based titania nanohybrids 3011
4. Conclusions 3012
   Acknowledgments 3012
   References 3012

ARTICLE INFO

Article history:
Received 1 April 2009
Accepted 12 June 2009
Available online 21 June 2009

Keywords:
Silica nanohybrid
Fluorescence
Gold nanoparticle
Quantum dots
Catalyst

ABSTRACT

Hybridized nanomaterials have been extensively investigated due to their superior properties over individual nanomaterials and molecules. Amorphous silica nanoparticles are often employed as a matrix or carrier, along with a functional component, to form a silica-based nanohybrid. The functional component can be a molecule or another type of nanomaterial. These nanohybrids combine the advantages employing both silica and the functional component. So far, a variety of applications of such nanohybrids has been reported. In this review, we have covered several major types of silica nanohybrids. The functional components include regular fluorophores, chemiluminescent molecules, drug molecules, quantum dots, gold nanomaterials, magnetic nanoparticles and nanocatalysts. The synthesis strategies, properties and potential applications of each silica nanohybrid are discussed in detail. A conclusion is drawn based on the current progress and future perspectives of the silica nanohybrids.

Published by Elsevier B.V.

* Corresponding author. Tel.: +1 701 777 3610; fax: +1 701 777 2331.
E-mail address: jzhao@chem.und.edu (J.X. Zhao).

0010-8545/$ – see front matter. Published by Elsevier B.V.
doi:10.1016/j.ccr.2009.06.005

1. Introduction

The rapid development of nanoscience and nanotechnology has produced a wide variety of novel nanomaterials. These nanomaterials overcome some of the limitations of bulk materials and have demonstrated great potential for various applications. However, each type of nanomaterial has its own drawbacks and limitations. Thus, direct use of the nanomaterials, without modification or functionalization, can be problematic. For example, most nanomaterials, including gold nanomaterials, magnetic nanoparticles and quantum dots, are difficult to directly and uniformly suspend in aqueous solutions. Furthermore, quantum dots and metal oxide nanomaterials become unstable in acidic environments. One option to overcome these limitations is to coat these nanomaterials with a more stable and physically adaptive material. Pure amorphous silica nanomaterials suffer from similar limitations and are also rarely employed alone for practical applications. However, when amorphous silica nanomaterials are hybridized with functional molecules or another nanomaterial, their applications extend broadly to bioimaging, biosensing, drug delivery, cancer therapy and catalysis.

Silica nanomaterials have several important properties that make them a unique matrix for incorporating functional components. First, the high porosity of amorphous silica nanoparticles provides the three dimensional space required for the doping of functional components, known as the dopants. The porosity is sufficiently adjustable to hold small molecules or large nanomaterials. The dopants can be easily embedded inside a silica shell or attached on a silica nanoparticle surface through chemical binding or physical adsorption. Second, silica nanomaterials are effectively "transparent". They are unlikely to absorb light in the near-infrared, visible and ultraviolet regions or to interfere with magnetic fields, which allows the dopants inside silica matrix to keep their original optical and magnetic properties. Third, the silica matrices are nontoxic and biocompatible for biomedical research. Finally, the well-established silica chemistry facilitates the modification of silica-based nanohybrids.

Silica nanohybrids are formed by a variety of methods. Functional molecules, such as fluorophores, drug molecules and photosensitizers, are most often immobilized inside the silica during the synthesis of silica matrix. Less commonly, functional molecules are immobilized on the surface of silica nanoparticles. The decoration step, in which functional molecules are immobilized, follows the formation of the pure silica nanoparticles. The surfaces of silica nanoparticles are usually functionalized with amine or carboxyl groups prior to the decoration.

The introduction of functionalized materials into silica nanoparticles adds new properties to the hosts, such as fluorescence, magnetism, therapeutic ability and catalytic function. Furthermore, silica nanoparticles not only provide shelters for dopants, but also enhance or ameliorate their intrinsic properties. For example, entrapped fluorophores exhibit a higher quantum yield and a stronger photostability than free ones. The release rate of drug molecules can be regulated once loaded inside the silica matrix. The toxicities of quantum dots and metal nanoparticles are suppressed under the protection of silica shells. Moreover, silica nanomaterials are a good scaffold for designing multifunctional nanomaterials which can accomplish multiple tasks simultaneously.

Functionalized silica nanomaterials have been summarized in previous reviews [1–5]. The emphasis of this article is the hybridization of silica nanoparticles with other functional nanomaterials and molecules. In each section, the synthesis of the silica nanohybrids is summarized at the beginning, followed by their unique properties and applications. Finally, a perspective of likely future directions of silica nanohybrids is provided.

2. Molecule–silica nanohybrids

A wide variety of functional molecules have been doped into silica nanoparticles to form molecule–silica nanohybrids. The associations between molecules and silica matrices are varied. A common linking force is electrostatic interaction between the negatively charged silica matrix and positively charged functional molecules. Covalent binding is frequently employed as well, which provides more stable hybrids but requires additional chemical reactions. The properties of individual functional molecules usually remain constant in the nanohybrids. However, due to the usually large number of molecules assembled into the small domain of a silica nanoparticle, some properties of trapped molecules can be enhanced in nanohybrids. These nanohybrids also have a more extensive array of applications than the molecules in their bulk state. Significant applications in the biological field include bioimaging, biosensing, drug delivery and cancer therapy. In this section, three types of molecule–silica nanohybrids used in these applications are discussed.

2.1. Fluorescent nanohybrids

The biological world has been brightened by the advent of fluorescence technology. With the assistance of fluorescent materials as tags, many biological processes are visualized under a fluorescence microscope and trace amounts of biological analytes are determined in living systems. However, individual fluorophore molecules, which are the most popular fluorescent labels for bioimaging and biosensing, have two major shortcomings: low fluorescence intensity and poor photostability. These problems significantly limit further applications of individual fluorophores as labels in the biological field. To overcome these limitations, silica nanoparticles have been employed as a matrix to produce silica-based fluorescent nanoparticles. By doping thousands of fluorophore molecules into a single silica nanoparticle, highly photostable and intense fluorescent molecule–silica nanohybrids have been developed, providing a revolutionary breakthrough for generating novel fluorescent tags [1–5]. A number of experiments have demonstrated that fluorescent silica nanoparticles are excellent substitutes for traditional, individual fluorophores in biological and biomedical applications.

2.1.1. Synthesis

In general, fluorescent molecules are doped inside silica nanoparticles by electrostatic interactions between the dye molecules and the silica matrix. Fluorophores can also be immobilized onto the silica nanoparticle surface through chemical reactions. When fluorophores are doped inside silica nanoparticles, the doping process should take place during the synthesis of the nanoparticles. This is most easily accomplished by using a Stöber or a reverse-microemulsion method of synthesis.

In the Stöber method, silica nanoparticles are produced by the hydrolysis and polymerization of a precursor, tetraethylorthosilicate (TEOS) [6]. A significant number of fluorophore molecules are doped into the silica matrix when they are pre-conjugated with a second precursor and allowed to co-polymerize with TEOS. Pre-conjugation of the fluorophore with the second precursor usually is achieved through covalent bonding. For example, (3-aminopropyl) triethoxysilane (APTS) is a precursor which contains a primary amine. A number of amine-reactive fluorophores have been successfully coupled to APTS [7]. Using this strategy, multicolored silica nanoparticles that produce efficient fluorescent resonance-energy transfer (FRET) were developed by adding several fluorophore–APTS conjugates during polymerization [8]. The amount of fluorophore molecules per silica nanoparticle can be adjusted simply by changing the ratio of TEOS to the

fluorophore–APTS conjugate. The size of silica nanoparticles is adjustable as well, as it is affected by the precursor concentration and polymerization time. The increase of precursor concentration and reaction time generally leads to a larger sized silica nanoparticle.

Fluorescent silica nanoparticles can also be produced by a reverse microemulsion approach (Scheme 1) [9–14]. A typical reverse microemulsion is composed of a relatively large amount of an organic solvent; a small amount of water; surfactant; and a catalyst, typically ammonium hydroxide. The water is dispersed into numerous nanometer sized water droplets within the organic phase and stabilized by the surfactant links to form a transparent microemulsion. TEOS enters the water droplets and is polymerically hydrolyzed. For this reason, the size and shape of silica nanoparticles produced by the reverse microemulsion approach are mainly dictated by factors affecting the initial drop size – ratio of water to surfactant, type of organic solvent and surfactant – although the amount of TEOS has some effect as well [9,11]. Recently, a method based on composition of the organic phase of the reverse microemulsion was developed to systematically change silica nanoparticle size over a continuous spectrum [9].

To efficiently dope fluorophore molecules into silica nanoparticles by the reverse microemulsion approach (Scheme 1, Route a), water solubility is required for the fluorophores or fluorophore–precursor conjugates so they will remain primarily in the aqueous phase. During the polymerization of TEOS, the silica nanoparticles grow and embed fluorophores simultaneously. However, the fluorophores can leak out of the silica nanoparticles if associations between the fluorophore and the silica matrix are weak. This is especially true for physically doped fluorophores. For these nanohybrids, positively charged fluorophores have a distinct advantage of remaining entrapped within the negatively charged silica matrix through electrostatic interactions. For example, the inorganic fluorophore, tris(2,2′-bipyridyl) ruthenium(II) chloride hexahydrate ($[Ru(bpy)_3]^{2+}$), is stably doped inside the silica matrix [11,12]. Likewise, the water-soluble organic fluorophore, dextran conjugated tetramethylrhodamine, can only be trapped inside the silica matrix when it is positively charged [13]. Without complementary electrostatic interactions, covalent binding between the silica matrix and the fluorophore must be employed, usually by introducing a second precursor–fluorophore conjugate prior to the polymerization.

The immobilization of fluorophores onto the silica nanoparticle surface is another strategy to form fluorophore-silica hybrids [15–18]. In this case, a pure silica nanoparticle is first prepared using the Stöber or reverse microemulsion method. Then, a second precursor containing amine or carboxyl groups, such as APTS or *N*-(trimethoxysilylpropyl)-ethylenediamine triacetic acid trisodium salt, is introduced to the microemulsion. The polymerization of the second precursor results in a silica surface with reactive groups of amine or carboxylic acid, which provide surface binding sites for conjugation of fluorophores (Scheme 1, Route b).

The number of fluorophore molecules per silica nanoparticle determines fluorescence intensity of the nanohybrid. High fluorophore concentration in the aqueous phase during synthesis leads to intensely fluorescent nanoparticles. However, if the fluorophore concentration exceeds a certain limit, self-quenching will occur. Thus, the fluorescence intensity of nanoparticles is adjustable by changing fluorophore concentration within a certain range.

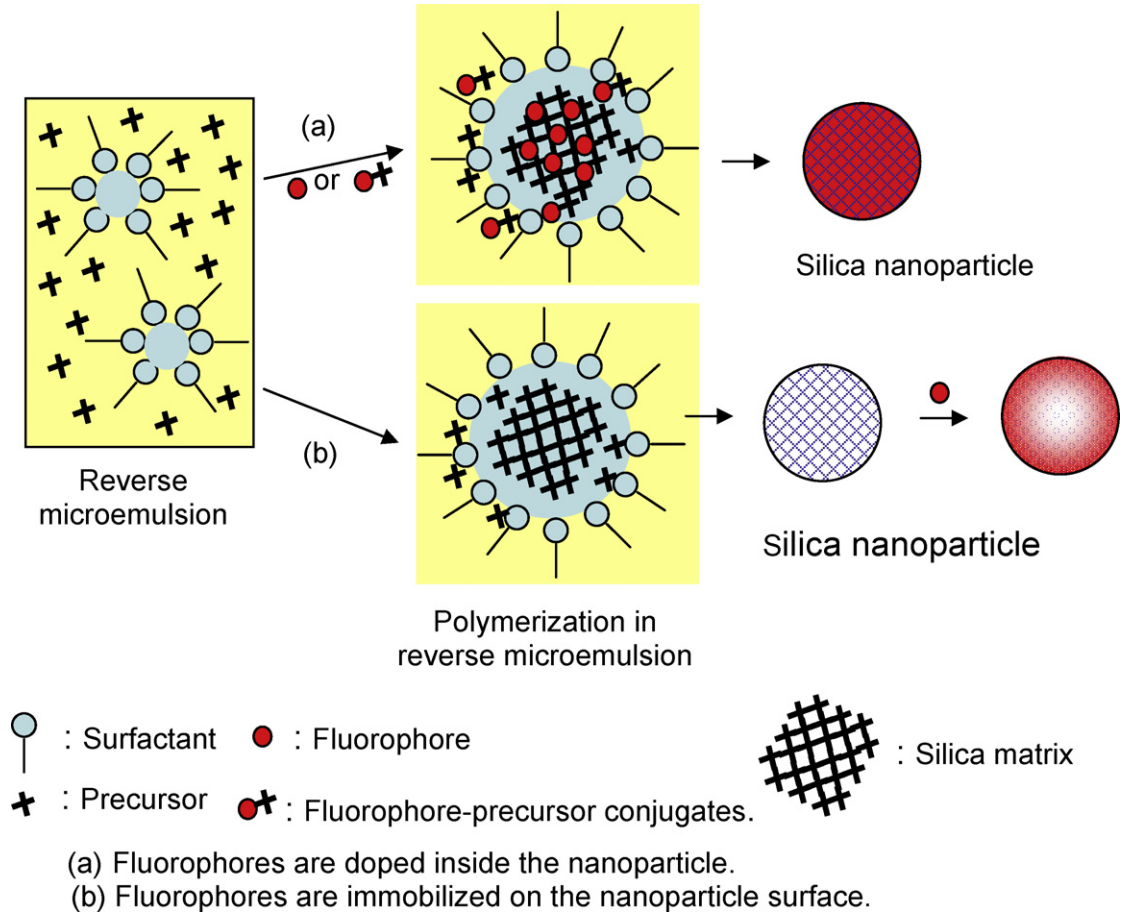

Scheme 1. Synthesis of fluorescent silica nanoparticles by a reverse microemulsion approach.

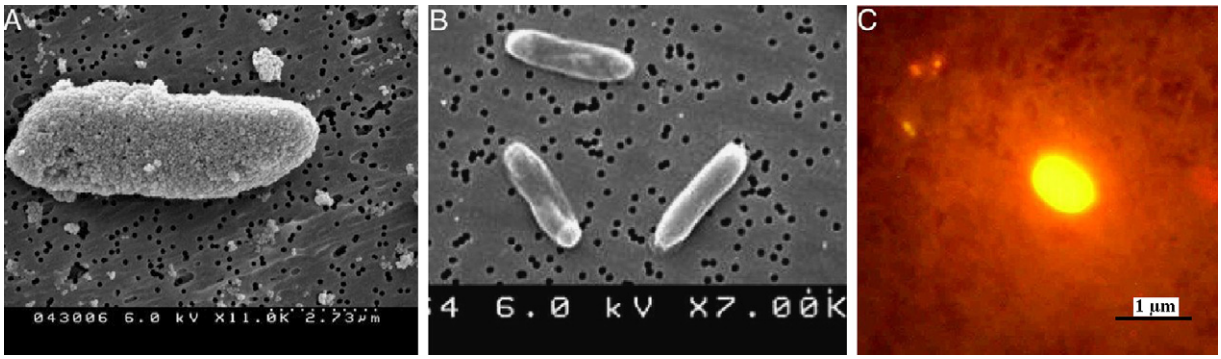

Fig. 1. Determination of *E. coli* 157 using fluorescent silica nanoparticles. (A) SEM image of a single *E. coli* 157 cell bound with fluorescent silica nanoparticles. (B) Control bacterial cells of *E. coli DH* 5α. (C) The fluorescence image of a single *E. coli* 157 cell bound with fluorescent silica nanoparticles. Reproduced with permission from Ref. [21].

2.1.2. Properties and applications

Fluorescent silica nanohybrids offer several key performance advantages compared with individual molecular fluorophores. These include more intense fluorescence emission, greater photostability and good biocompatibility. While all three offer great advantages for biological applications, it is important to note that these improved performance characteristics are generated primarily from hybridization with the silica nanomatrix.

The relative intensity of a fluorescent silica nanoparticle is much higher than that of an individual fluorophore. A single fluorescent silica nanoparticle can contain thousands of fluorophore molecules. Thus, the fluorescence intensity of one nanoparticle is arguably thousands of times higher than that of one fluorophore. Moreover, the quantum yield of a fluorophore can be enhanced by embedding it within the silica matrix because non-radiative decay is reduced in this less polar and more restrictive environment [19,20].

The high photostability of the nanoparticle originates from protection the silica matrix provides for the embedded fluorophores. Environmental oxygen is a universal quencher for fluorophores in aqueous solution and the network structure of the silica matrix reduces diffusion of environmental oxygen to fluorophores. Thus, the photostability of embedded fluorophores is greatly improved [13].

The fluorescent silica nanoparticles have shown great potential as fluorescence labeling materials for the determination of a variety of analytes ranging from small ions and molecules to large marcomolecules and cellular samples. When the silica surfaces are modified with a recognition component for biological targets, such as antibodies or single-strand DNA molecules, the target cells or complementary DNA can be determined. For example, fluorescent silica nanoparticles functionalized with antibodies against *Escherichia coli* 157: H7 were employed for the determination of bacterial cell of *E. coli* 157 (Fig. 1) [21]. A single bacterial cell was detected without traditional signal amplification. Furthermore, multiple bacterial cells were determined simultaneously using multiple colored silica nanoparticles [22]. Additionally, aptamer-conjugated fluorescent silica nanoparticles were able to indentify target cancer cells, such as Human T cell lymphoblast-like cell line (CCRF-CEM), Ramos and Toledo cancer cells [23]. Instead of targeting a whole cell, fluorescent silica nanoparticles can also detect single-strand DNA molecules when a complimentary DNA strand was immobilized onto fluorescent silica nanoparticles [24].

In addition to the macrobiomolecules, a number of small ions and molecules have been determined using fluorescent silica nanoparticles. For example, a pH sensitive fluorophore, fluorescein isothiocyanate (FITC), was covalently embedded in the silica nanoparticles together with a pH insensitive fluorophore, tetramethylrhodamine isothiocyanate (TRITC), as a reference. The fluorescence intensity ratio of FITC to TRITC changed as the pH varied. Thus, the H^+ concentration in the environment was measured [25]. Using the same strategy, Ca^{2+}, Mg^{2+}, Zn^{2+} and O_2 were determined using fluorescent dye-doped silica nanoparticles [26–28]. The nanoparticles can be delivered into cells and probe the concentrations of ions and molecules inside the cells.

The surface immobilized fluorophore silica nanoparticles can give a quick response when used for ion determination. When a zinc ion sensitive ligand, 6-methoxy-8-*p*-toluenesulfonamidequinoline, was immobilized on silica nanoparticle surfaces, the fluorescent signal increased dramatically in presence of zinc ions [16].

Fluorescent silica nanoparticles have also demonstrated advantages for the indirect determination of ions and molecules vicinal to the nanoparticles. The common pathway involves a target molecule or ion complex which transfers or absorbs the fluo-

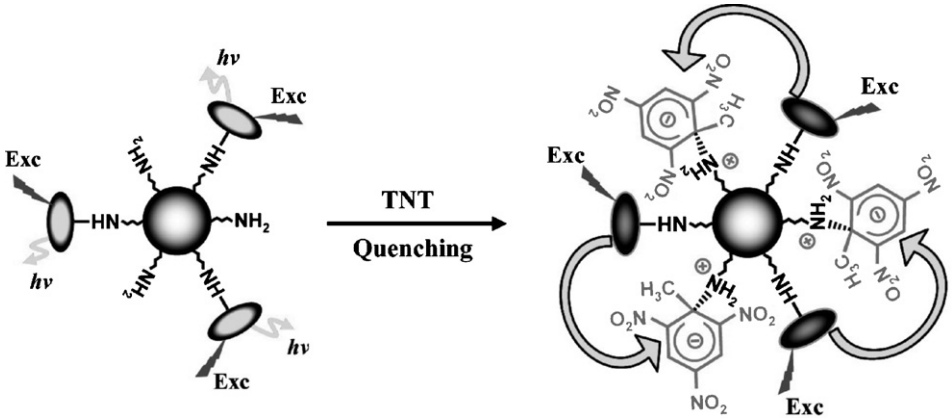

Fig. 2. Determination of TNT molecules by fluorescent silica nanoparticles via a fluorescence quenching mechanism. Exc = excitation. Reproduced with permission from Ref. [17].

rescent energy from the nearby fluorophores inside the silica nanoparticles, resulting in changes of fluorescence intensities of the nanoparticles. The intensity change is proportional to the target ion/molecule concentration. For instance, an ultrasensitive detection of 2,4,6-trinitrotoluene (TNT) was developed based on fluorescence quenching of a fluorescent silica nanoparticle (Fig. 2) [17]. First, silica nanoparticles were modified with amine groups using APTS. Then, the fluorophore (FITC or 6-carboxy-X-rhodamine *N*-succinimidyl ester (ROX)) was immobilized on the silica nanoparticle surface. Finally, the TNT bound to the amine group on the nanoparticle surface and absorbed energy from the nearby FITC via fluorescence energy transfer, resulting in quenching of the fluorescence signal. The detection limit reached 1 nM TNT in solution and several ppb of TNT vapor in air. By a similar method, Pb^{2+} and Ni^{2+} ions were determined [29,30].

In summary, silica nanoparticles can be hybridized with fluorophore molecules through chemical binding or physical interaction either on the nanoparticle surface or within the nanoparticle matrix. In the resulting hybrid, the silica functions as a matrix and a carrier to protect and deliver fluorophores. Typically, the function of the fluorophore is a signal probe for the determination or detection of specific targets. Their combination produces a photostable, intense and biocompatible fluorescent nanoparticle for sensitive determination of a wide variety of targets ranging from ions to cells and tissues.

2.2. Chemiluminescent nanohybrids

The two major attractive features of chemiluminescence (CL) are low background signals and the simple, inexpensive instrumentation it requires. In CL, excited species are produced by the energy released in a chemical reaction. The reaction can be manipulated to give luminescent signals related to an analyte concentration. Unlike photoluminescence measurements, CL requires no external radiation source. Thus, it not only eliminates the need for an intense, stable source of light, but also results in a low background signal. However, the low intensity of most CL signals largely limits its applications in trace analysis.

To take full advantage of CL in trace analysis, enhancement of the CL signal is greatly needed. The recent development of chemiluminescent nanoparticles provides a new solution for concentrating CL-producing species in the small domain of a nanoparticle. It has been reported that the hybrids of chemiluminescent molecules with silica nanoparticles are efficient luminescent probes for the sensitive determination of trace analytes. The synthesis of chemiluminescent silica nanoparticles is similar to the approach of making fluorescent silica nanoparticles as described in Section 2.1.1, but instead of doping fluorophores, CL-producing lumophores are doped into the silica nanoparticles.

Two types of chemiluminescent silica nanoparticles have been reported. One was doped with luminol and the other was doped with $[Ru(bpy)_3]^{2+}$. Although both luminol and $[Ru(bpy)_3]^{2+}$ give direct fluorescence signals, they also can undergo chemiluminescence processes. In particular, these two CL reagents have been proven to be very useful in electrogenerated chemiluminescence (ECL) applications [31,32]. Their ECL pathways are described as below.

2.2.1. Chemiluminescence pathways

The CL pathways of $[Ru(bpy)_3]^{2+}$ and luminol in silica nanoparticles are similar to those in aqueous solution. The electrochemically produced tripropylamine (TPA) radical, is a suitable co-reactant for the production of $[Ru(bpy)_3]^{2+}$ ECL. First, $TPA^{\bullet+}$ and $TPA^{\bullet}$ are produced readily in TPA solution by applying a positive potential bias to an electrode (Eqs. (1) and (2)). Then, $[Ru(bpy)_3]^{2+}$ is reduced to $[Ru(bpy)_3]^{+}$ by $TPA^{\bullet}$ (Eq. (3)). The radical cation, $TPA^{\bullet+}$, oxidizes

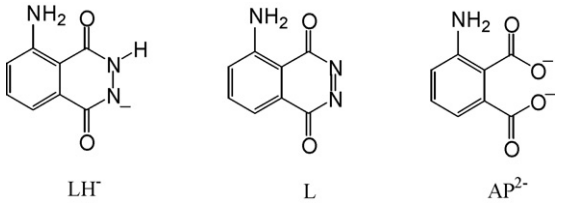

Scheme 2. Structures of luminol derivatives.

$[Ru(bpy)_3]^{+}$ to yield $[Ru(bpy)_3]^{2+}$ in its excited state (Eq. (4)) [31]. Notably, $[Ru(bpy)_3]^{2+}$ is regenerated easily (Eq. (5)), so the reaction can be carried out continuously as long as a supply of TPA or another co-reactant remains. This characteristic makes $[Ru(bpy)_3]^{2+}$ exceptionally useful in a sensor platform.

$$TPA \rightarrow TPA^{\bullet+} + e^- \quad (1)$$

$$TPA^{\bullet+} \rightarrow TPA^{\bullet} + H^+ \quad (2)$$

$$TPA^{\bullet} + [Ru(bpy)_3]^{2+} \rightarrow [Ru(bpy)_3]^{+} + TPA^{+} \quad (3)$$

$$[Ru(bpy)_3]^{+} + TPA^{\bullet+} \rightarrow [Ru(bpy)_3]^{2+*} + \text{products} \quad (4)$$

$$[Ru(bpy)_3]^{2+*} \rightarrow [Ru(bpy)_3]^{2+} + h\nu \quad (5)$$

The CL process of luminol usually requires a metal catalyst [32]. However, its electrogenerated chemiluminescence pathway (Eqs. (6)–(8)) requires no catalyst. Luminol exists in solution as a form of LH^- (Scheme 2) which can be electrochemically oxidized to its more reactive form of L (Eq. (6)). This specie will react with an oxidant such as hydrogen peroxide to yield AP^{2-} in its excited state (Eq. (7)). Once this reaction occurs, regeneration of luminol is unlikely [32].

$$LH^- \rightarrow L + H^+ + 2e^- \quad (6)$$

$$L + H_2O_2 \rightarrow AP^{2-*} + N_2 + 2H^+ \quad (7)$$

$$AP^{2-*} \rightarrow AP^{2-} + h\nu \quad (8)$$

2.2.2. Properties and applications

Chemiluminescent silica nanoparticles have been used both as sensor platforms and labels (Table 1). $[Ru(bpy)_3]^{2+}$ is particularly useful in sensor platforms due to its ability to regenerate. Electrogenerated chemiluminescent properties of $[Ru(bpy)_3]^{2+}$-doped silica nanoparticles were first demonstrated in the determination of TPA [34] with the assistance of a glassy carbon electrode (GCE). The ECL silica nanoparticles were immobilized on the GCE in a chitosan film. The non-conductive property of silica nanoparticles has been a problem for electrochemical measurement. To further improve conductivity of ECL sensor platforms made from silica ECL nanoparticles, carbon nanotubes [35] and gold nanoparticles [36] have been used to facilitate electron transfer in the modified sensors.

Although TPA is often used as a model analyte for $[Ru(bpy)_3]^{2+}$ sensing platforms due to its highly reactive electrochemically produced radical, its detection is of little practical use. Existing application-oriented publications describe $[Ru(bpy)_3]^{2+}$-doped silica nanoparticle as sensors for analysis of drugs in biological samples such as urine and serum. This application is important for establishing appropriate doses of new medicines [37]. A recent article has reported the detection of itopride in human serum with a $[Ru(bpy)_3]^{2+}$-doped silica nanoparticle/chitosan film on a GCE [37]. A similar sensor with the nanoparticles immobilized in a Nafion® film was used to detect metoclopramide in urine [38]. It is noteworthy that both of these analytes contain a tertiary amine group which is the reason they can be detected by this ECL method.

Sensor platforms containing luminol-doped silica nanoparticles have also been reported. To detect pyrogallol, luminol-doped silica nanoparticles were immobilized in a chitosan film on a graphite electrode as a sensor platform [42]. When pyrogallol was electrochemically oxidized, it reacted with oxygen to form an oxygen

Table 1
Chemiluminescent silica nanoparticles (NPs) used in chemical analysis.

NP dopant	NP role	Analyte	LOD, M	Linear range, M	Ref.
R	Sensor	TPA	5.0×10^{-8}	5×10^{-7} to 1×10^{-3}	[33]
R	Sensor	TPA	2.8×10^{-9}	9×10^{-9} to 8×10^{-5}	[34]
R	Sensor	TPA	2.8×10^{-9}	9×10^{-9} to 8×10^{-4}	[35]
R	Sensor	TPA	5.2×10^{-9}	6×10^{-8} to 1×10^{-4}	[36]
R	Sensor	Itopride	3.0×10^{-9}	1×10^{-8} to 2×10^{-5}	[37]
R	Sensor	Metoclopramide	7.0×10^{-9}	2×10^{-8} to 1×10^{-5}	[38]
R	Label	Thrombin	1.0×10^{-15}	1×10^{-14} to 1×10^{-11}	[39]
R	Label	DNA	1.0×10^{-13}	2×10^{-13} to 2×10^{-9}	[40]
L	Label	DNA	2.0×10^{-12}	5×10^{-12} to 1×10^{-9}	[41]
L	Sensor	Pyrogallol	1.0×10^{-9}	3×10^{-9} to 2×10^{-5}	[42]
L	Reagent	Isoniazid	1.5×10^{-10}	7×10^{-10} to 7×10^{-6}	[43]

R: $[Ru(bpy)_3]^{2+}$, L: luminol.

radical which in turn oxidized luminol in a highly energetic reaction that produced the excited state of AP^{2-}. The light output was then proportional to the concentration of pyrogallol. Despite irreversibility of the photoluminescence process, luminol-doped silica nanoparticles are not immediately exhausted of their luminol supplies. The sensor only lost 5% of its signal after 100 ECL experiments, and was therefore deemed stable enough for practical use [42]. A similar mechanism was also exploited to detect isoniazid-electrochemically oxidized isoniazid also reacted with dissolved oxygen to form the oxygen radical. However, in this case the nanoparticles were in the bulk of solution instead of being part of a sensor platform, perhaps a necessity due to the inability to reuse such a sensor [43].

Chemiluminescent nanoparticles may also be used as labels when their surfaces are modified with selective species such as antibodies or DNA. However, several layers of such modifications greatly hinder the electrogenerated chemiluminescent reactions [44]. In an investigation of the effect of polyelectrolyte and biomolecule modifications on the ECL signals of $[Ru(bpy)_3]^{2+}$-doped silica nanoparticles, each layer of modifiers decreased the signal by roughly 50% [44].

Nevertheless, there are several examples of either $[Ru(bpy)_3]^{2+}$- or luminol-doped silica nanoparticles as labels for specific biomolecular recognition. In what is perhaps the earliest example, a luminol-doped silica nanoparticle was used for the detection of a specific DNA sequence [41]. The target DNA sequence was immobilized on a poly(pyrrole)-modified platinum electrode, while the complementary probe DNA sequence was electrostatically bound to the nanoparticles whose surface was modified with chitosan. A detection limit of 2.0 pM was achieved with this method [41].

Later, a $[Ru(bpy)_3]^{2+}$-doped silica nanoparticle was employed to detect the same DNA target [40]. An improved detection limit of 0.1 pM was achieved which could be attributed to the superior ECL reagent. The excellent ECL behavior of $[Ru(bpy)_3]^{2+}$-doped nanoparticle was also demonstrated in the detection of thrombin. A thrombin aptamer was first immobilized on a gold electrode through an Au–thiol bond. Then, the nanoparticles were modified with a DNA sequence that was complimentary to the aptamer. When adding the nanoparticles to the electrode solution, its surface DNA hybridized to the thrombin aptamer. However, in the presence of thrombin, the nanoparticles were expelled from the electrode surface causing a decrease in ECL signal. The signal decrease could quantify the amount of thrombin present [39].

In summary, chemiluminescent silica nanoparticles have great potential for highly sensitive determination of trace analytes. However, the research thus far has seen much repetition and redundancy using only $[Ru(bpy)_3]^{2+}$ and luminol. This is likely due to the limited number of chemical species that undergo a chemiluminescent reaction. The field is in need of development of new chemiluminescent and electrochemiluminescent materials.

2.3. Drug transporting nanohybrids

Modern medicine requires drug carriers that have quick, target-oriented delivery and a controllable release rate. There has always been a great need for the development of suitable carriers for various medicines. To be an effective drug carrier, several basic properties are necessary: (1) low-toxicity and biodegradability; (2) the ability to encapsulate and release drug molecules; (3) specific surface functionality. So far, amorphous silica nanoparticles have proven to be nontoxic and to have an easily modified surface. Because of these properties, silica nanoparticles have been increasingly scrutinized for drug delivery and photodynamic therapy (PDT).

2.3.1. Synthesis

Similar to the synthesis of fluorescent silica nanoparticles, the doping of drug molecules inside the silica matrix can be achieved through either the reverse microemulsion or Stöber methods. However, unlike fluorophores and chemiluminescent molecules that are permanently doped, most drug molecules should be trapped only temporarily inside the silica matrix and should be easily released. Therefore, drug molecules are generally doped by physical means rather than chemical binding. Physical trapping, as by electrostatic attraction between the silica matrix and the dopant, is relatively weak and easily dissociated compared to chemical bonds.

The great challenge in nanohybrid syntheses of drug carriers is the low aqueous solubility of many drug molecules. Neither the reverse microemulsion method nor the Stöber method is able to efficiently incorporate hydrophobic molecules into the silica nanoparticle matrix. To solve this problem, organically modified silica (ORMOSIL) nanoparticles have been developed recently [45–49]. Hydrophobic drugs are first dissolved in the organic phase in the reverse microemulsion composing of dimethyl sulfoxide, sodium 1,2-bis(2-ethylhexoxycarbonyl) ethanesulfonate, butanol and water. With this unusual microemulsion composition, hydrophobic drugs are able to partition more effectively into the aqueous water droplets and are more efficiently trapped inside the silica nanoparticles by hydrolysis of the silane precursor, triethoxyvinylsilane.

The chemical/physical activities of silica nanoparticles are mostly based on their surface properties. Proper surface modification of the silica nanoparticles improves their drug delivery capability and efficiency. In general, the surfaces of silica nanoparticles are modified with specific functional groups of biomacromolecules by chemical binding or physical adsorption [50,51]. A typical modifier is an antibody molecule decorating a carboxyl-functionalized silica nanoparticle. The carboxyl groups on the silica surface form amide bonds with the primary amine groups in antibodies [3]. The immobilized antibody can then more effectively vector the nanoparticle toward a particular tissue or cell type. The formation of disulfide bonds is also an effective chemical

binding approach to immobilize recognition elements [3]. However, physical adsorption of biocompatible macromolecules onto silica nanoparticle surface is often the most simple and efficient method for immobilization. The electrostatic forces readily drive many macromolecules, such as poly(ethylene glycol) (PEG), proteins and lipids, to physically adsorb to the nanoparticle surface that can be decorated with variety of functional groups [50,51].

In addition to solid-core silica nanoparticles, hollow silica nanoparticles have also been employed as drug carriers [52–55]. Compared to the solid-core silica nanoparticles, the hollow counterparts possess much higher loading capacity for drug molecules but weaker interactions between the drug molecules and the silica matrix, making controlled release more problematic. There are two main synthetic methodologies for hollow silica nanoparticles. The first method is template-based synthesis [52–58]. The second method uses a dissolution-regrowth process of solid silica nanoparticles (Fig. 3) [59,60]. The first method generally utilizes a solid nanoparticle composed of metal [55], metal oxide [53,54,57,58] or polymer [52,56] as a core template. The silica shell is then grown on the template and the core is removed by an etching process, dissolution or calcination. The second method is relatively simple since the hollow cores are produced by etching the regular silica nanoparticles using bases, such as sodium hydroxide (NaOH) or sodium borohydride ($NaBH_4$) [59,60]. Polyvinylpyrrolidone molecule (PVP) on the silica nanoparticle surfaces provides protection. Thus, the inner part of silica nanoparticle is selectively etched. This etching process takes place over a time period of hours to days [59,60].

2.3.2. Properties and applications

The characterization of drug molecule–silica nanohybrids has provided a foundation for applications of silica nanoparticles as a drug carrier. So far, characterization has been limited to several fundamental aspects which include doping efficiency, uptake by living systems, dopant release, and dopant effects upon release. Nevertheless, these characterizations have suggested new applications for drug delivery and a wider range of drug-based nanohybrid materials.

Doping efficiency of drug molecules in the silica matrix has generally been characterized by UV–vis spectroscopic measurements and fluorescence spectrometry [48,49,54]. UV–vis spectra can easily monitor the amount of doped drugs since the majority of drugs contain aromatic structures. When the dopant is a photosensitizer, which is usually used for photodynamic therapy, fluorescence measurements are more sensitive. In fact, fluorescent molecules are often doped inside silica nanoparticles as a model for drug delivery investigation [55].

Characterization of nanohybrid uptake has focused on the ability of the nanoparticles to deliver their cargo within living systems. Most delivery methods have been studied *in vitro* rather than *in vivo* investigations. For *in vitro* studies, the delivery of fluorescent silica nanoparticles into cells can be tracked by fluorescence microscopy [9]. Endocytosis and phagocytosis are two major pathways by which cells take up silica nanoparticles. These processes are greatly affected by the nanoparticle sizes and surface properties. Smaller nanoparticles more easily penetrate the cell membranes than larger ones (Fig. 4) [9]. The surface modification can assist nanoparticles in being delivered to the specific target site. For example, surface modifications with antibodies and aptamers can improve the target recognition [61].

Release of drug molecules from silica nanohybrids, once the nanoparticles penetrate the cell membrane, has also been characterized. Kinetics of the drug-release have usually been monitored through the changes of the UV–vis and fluorescence spectra of silica nanohybrids [54], although high performance liquid chromatography has also been employed for drug-release kinetic measurements [58]. These investigations have demonstrated that many factors

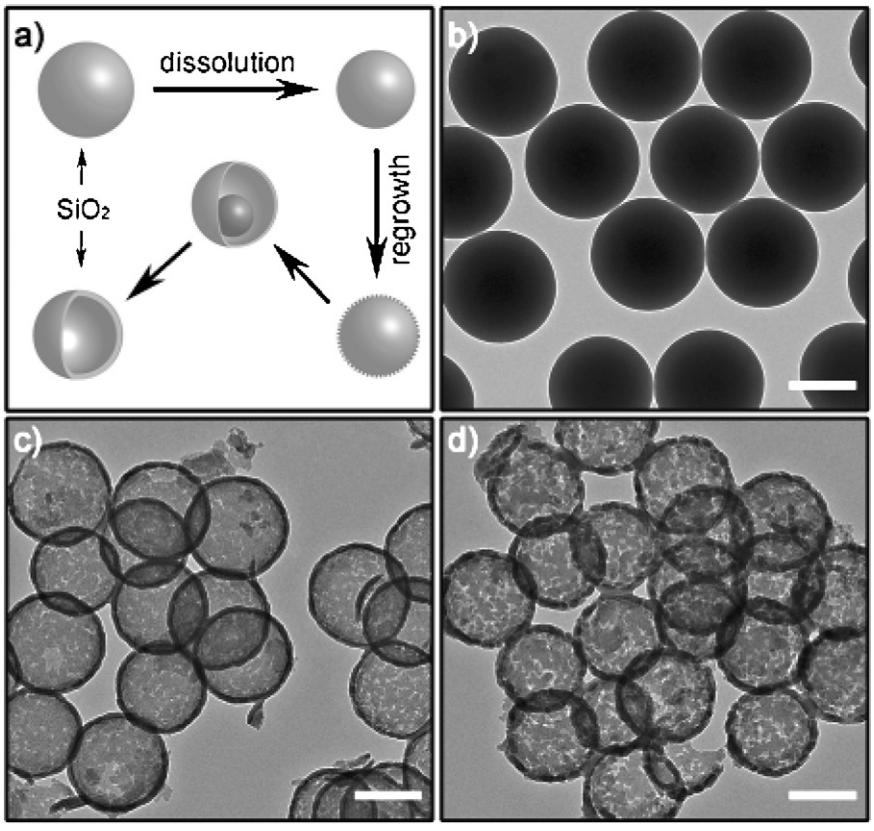

Fig. 3. Hollow silica nanoparticle formed through a dissolution-regrowth process. (A) Process for formation of hollow silica nanoparticles. (B) TEM image of solid silica nanoparticles. (C and D) TEM images of hollow silica nanoparticles prepared at different conditions. Scale bar: 200 nm. Reproduced with permission from Ref. [60].

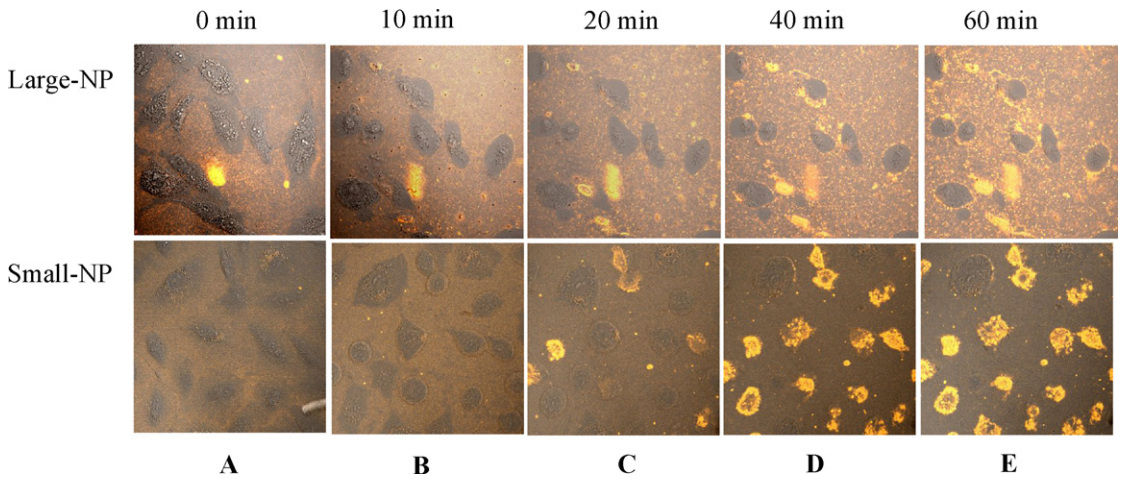

Fig. 4. Penetration of fluorescent silica nanoparticles to A549 cells monitored by a confocal fluorescent microscope. Large nanoparticles: 85 nm, small nanoparticles: 23 nm. Reproduced with permission from Ref. [9].

affected the rate of drug release. For hollow silica nanoparticles, the key factors include cavity size, shell thickness and type of surface functional groups. For example, PEG-coated hollow silica nanoparticles were found to release drug molecules at a much slower rate than the hydroxyl- and amine-functionalized hollow nanoparticles [54]. It was presumed that PEG on the surface partially blocked the silica nanoparticle pores, resulting in reduced porosity. In another study, it was found that thicker shells allowed a drug to be released at a slower rate and over a longer period of time [58]. The thicker silica shells also reduced the cavity size of the nanohybrid and concomitantly decreased drug-loading capacity. Meanwhile, the environmental conditions, such as pH and temperature, also influenced the release of drug molecules [53].

Some of the most illustrative characterization of drug nanohybrids have been based on treatment results. The cell proliferation assay is the preferred method for evaluation of the drug functions. With photodynamic therapy, for example, the survival percentage of the treated cells with photosensitizer-doped nanoparticles was dramatically reduced after cells were exposed to light [45,46,48]. Longer photo-irradiation and higher doses of photosensitizers inside the nanoparticles led to an increased death rate of the treated cells. In gene therapy studies, DNA molecules can be delivered to the target cells [47,62–64]. The expression of delivered DNA molecules is the sign of the successful gene delivery and transfection [47,49]. For example, the pEGFP-N2 vector, which can produce the green-fluorescent protein (GFP), was employed in Roy's gene delivery study (Fig. 5) [49]. The cellular fluorescence signal from the treated cells suggested the pEGFP-N2 was successfully delivered to the cells without losing its function.

The treatment result of photodynamic therapy using hybridized nanoparticles has been evaluated in a different manner. The principle of PDT is to use singlet oxygen produced by photosensitizers to kill malignant cells. Thus, accurate measurement of the produced singlet oxygen is crucial for evaluation of the photodynamic therapy. Usually, the generation of singlet oxygen can be directly monitored by its phosphorescence spectrum at 1270 nm [48,65]. Meanwhile, singlet oxygen can also be tracked by the indirect method, that is, the decrease of the fluorescence signal of 9,10-dipropionic acid, which is quenched by singlet oxygen [46,48,66]. The experimental results have demonstrated that photosensitizers retain their functions of generating singlet oxygen after being embedded inside the silica matrix [48]. The amount of singlet oxygen generated by the ORMOSIL nanoparticle-doped photosensitizers is comparable to that produced by the same amount of free photosensitizers. The lifetimes of singlet oxygen generated by both

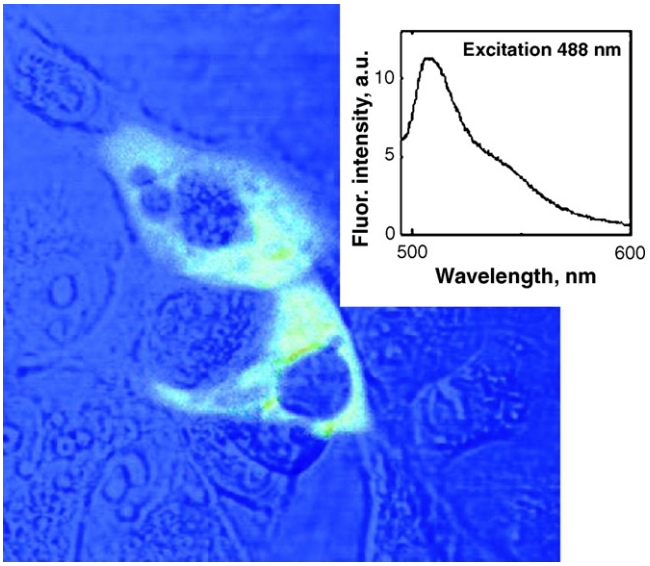

Fig. 5. A combined fluorescence and transmission image of COS-1 cells transfected with pEGFP delivered with silica nanoparticles. Inset spectrum is the fluorescence spectrum of EFGP taken from cell cytoplasm. Reproduced with permission from Ref. [49].

the free and doped photosensitizers are also similar [48]. In addition, when doped inside the silica matrix, the negative effects of photosensitizers, such as toxicity and hydrophobicity, are tremendously reduced.

In summary, the characterization of drug molecule–silica nanohybrids has demonstrated great potential for using these materials as efficient carriers for drug delivery. However, a number of medical and biological studies are still needed before effective clinical applications can be realized.

3. Functional nanomaterial-silica nanohybrids

Silica nanoparticles have been widely used as a matrix in which other functional nanomaterials are doped. Hybridization of the two types of nanomaterials overcomes some limitations of the individual nanomaterials and ultimately helps to bring nanotechnology from laboratorial studies to practical applications. Up to this point, such silica nanohybrids have had some impact in the fields of bioimaging, cancer therapy and catalysis. In this section, several

functional silica nanohybrids will be described, from their synthesis to their potential and realized applications.

3.1. Quantum dot nanohybrids

Quantum dots have been extensively studied because of their unique luminescent properties and great potential for biological applications [67–72]. As a result of the quantum size confinement effect, the narrow emission peaks in their luminescence spectra can be precisely tuned by adjusting their size. In addition, the luminosity of quantum dots is strong and resistant to photobleaching. Considering only these luminescent properties, quantum dots appear to be ideal candidates for bioimaging and biosensing [73–79]. From the perspective of biocompatibility, however, unmodified quantum dots demonstrate severe toxicity because they are generally composed of heavy metals and susceptible to release of these metals [80–88]. As such, the direct use of quantum dots in biological systems may cause undesirable side effects. Easer and safer use of quantum dots has been demonstrated by shielding them with silica layers [83]. Silica-modified quantum dots possess three major advantages. First, their toxicity is greatly reduced when coated with silica shells. Second, the quantum dot nanohybrids are much more stable against degradation, and third, they are readily modified with functional molecules or biomacromolecules.

3.1.1. Synthesis

The syntheses of quantum dot-silica hybrids are mostly based on the reverse microemulsion method [89–96] and the Stöber method [97–106]. In both cases, it is necessary to convert the quantum dots from hydrophobic to hydrophilic character prior to the growth of a silica shell because they need to be evenly suspended in a polar medium, such as alcohol or aqueous solution. A ligand exchange can effectively turn quantum dots hydrophilic and is usually the first step prior to coating (Scheme 3, Route 1). This is followed by transfer of the hydrophilic quantum dots to the silica growth solution. In the reverse microemulsion method, the growth of silica occurs inside the water droplets where the hydrophilic quantum dots are trapped [90]. The amount of quantum dots per water droplet is variable by changing synthetic conditions, such as the surface charge of the quantum dots and the type of precursor. In general, negatively charged quantum dots tend to form single-dot doped silica nanoparticles in the negatively charged silica matrix due to electrostatic repulsion. Multiple-dot doped silica nanoparticles are more likely to be produced when the surface of the quantum dots and the silica matrix hold opposite charges. For example, in a negatively charged silica matrix, the thioglycolic acid (negative charge) modified quantum dots formed single-dot silica nanoparticles, while in a positively charged matrix (e.g. silica matrix modified by the positively charged poly(diallyldimethyl ammonium chloride)) multiple-dot doped silica nanoparticles were produced [90].

Ligand exchange of quantum dots can also take place in the reverse microemulsion, where a variety of compounds such as surfactants and the hydrolyzed precursors can bind to the quantum dot surface [89–93,95,96]. This means that the whole process – including ligand exchange, the transfer of quantum dots to aqueous phase, and the growth of silica shells – can be accomplished in a one-pot synthesis (Scheme 3, Route 2) and the overall procedure is greatly simplified. However, the process might be slowed or even interrupted completely if the quantum dots are firmly bonded by hydrophobic ligands such as those with thiol groups [95]. In this case, surfactants and the hydrolyzed precursors are unable to replace the hydrophobic ligands. Consequently, the hydrophobic quantum dots cannot reach the aqueous phase and free silica nanoparticles form without a quantum dot core. The formation of quantum dot-doped silica nanoparticles is also influenced by the variation in the amount of quantum dots. An increase in quantum

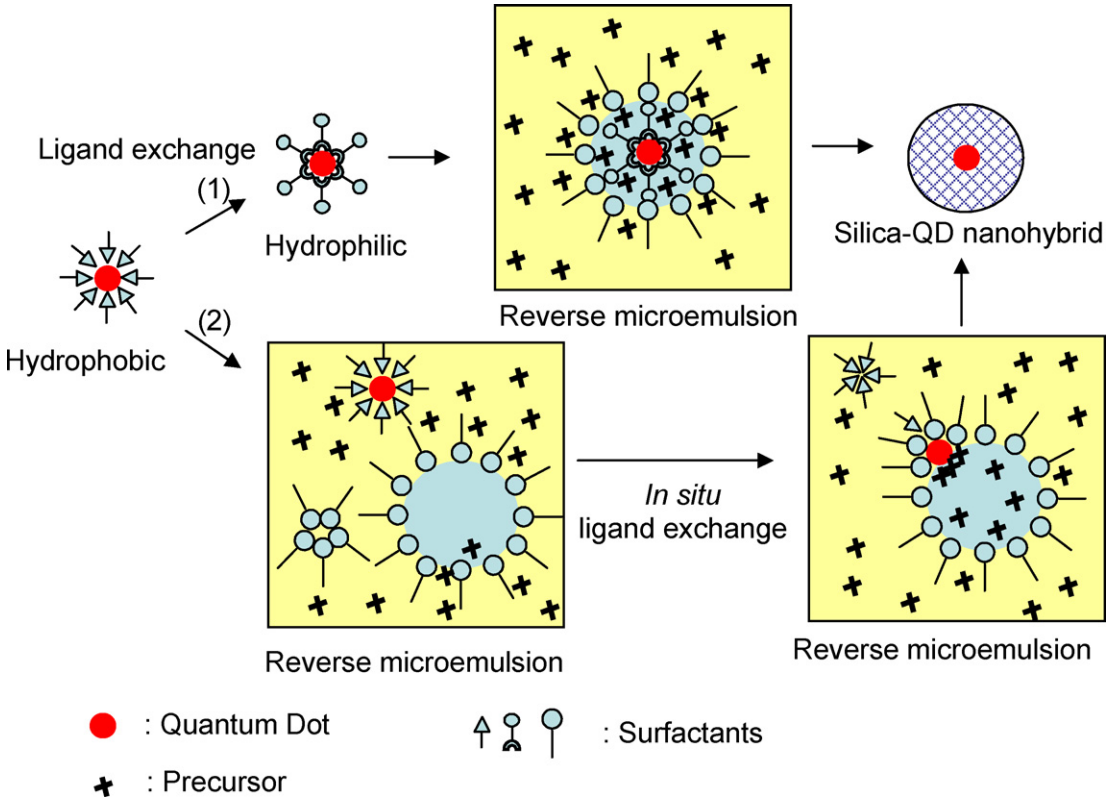

Scheme 3. Schematic diagram of the synthesis of silica-quantum dot nanohybrids by a reverse microemulsion method; (1) a sequential ligand exchanging route, and (2) an *in situ* ligand exchanging route.

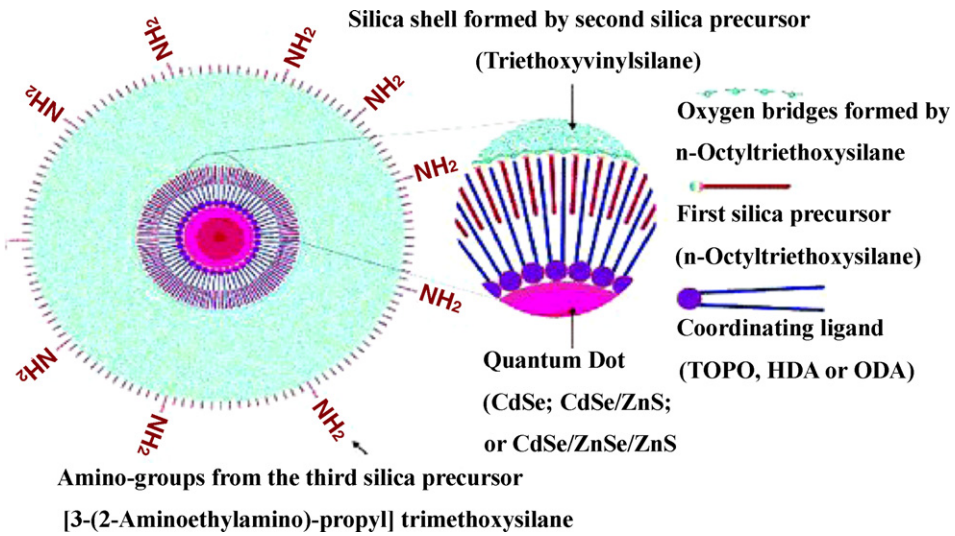

Scheme 4. A schematic model of a single quantum dot embedded in a silica matrix prepared without ligand exchanging. Reproduced with permission from Ref. [97].

dot loading can reduce the formation of silica nanoparticles without quantum dots. However, an excess amount of quantum dots can generate multiple-dot doped silica nanoparticles.

The Stöber method is also employed for synthesis of quantum dot-silica nanohybrids. The synthesis has two requirements: the quantum dots must be water soluble and the silica precursor must be able to adhere and grow on the quantum dot surfaces. The first requirement can be met by proper ligand exchange as described previously. The second requires a functional precursor, such as APTS or (3-mercaptopropyl)trimethoxysilane (MPTS), which adhere to the surface of quantum dots. TEOS can also be made to adhere and form the silica layer if the surface of quantum dots is first modified with PVP and cetyltrimethylammonium bromide (CTAB) [103]. With this as well as the reverse microemulsion methods, the thickness of the silica shell outside the quantum dot-core can be controlled by varying the amount of silica precursors. Different surface functional groups can also be introduced to the silica shell by the addition of the functionalized precursors.

All the methods described above require the replacement of the quantum dot surface ligands, which causes a reduced luminescence quantum yield. To circumvent this problem, a modified Stöber-based method that can directly coat silica layer on hydrophobic quantum dots was developed (Scheme 4) [97,105,106]. In this method, a hydrophobic precursor, *n*-octyltriethoxysilane, was first coordinated to the hydrophobic quantum dots. Precursors of triethoxyvinylsilane and APTS were then added to form the silica layers that surround the unchanged quantum dots. Using this method, the majority of the quantum dots (92%) form single-dot silica nanoparticles with nearly 70% of their fluorescence quantum yield preserved [97].

3.1.2. Properties and applications

The primary goal of silica coating is to reduce the toxicity of quantum dots. The toxicities of quantum dots are manifested in a several different ways. First, the oxidizing surfaces of quantum dots generate reactive oxygen species which cause cell death. Second, toxic heavy metal ions can be released from quantum dots, such as Cd^{2+} [81,82,86,87]. Both of these pathways require oxygen or other reactive species to directly contact the surface of the quantum dots. In that sense, the isolation of quantum dots from the local environment can effectively reduce their toxicity. Silica nanoparticles, which themselves are well known to be nontoxic nanomaterials [107], are effective blocking materials for quantum dots. Current studies show that a silica shell can effectively reduce or even eliminate the toxicities of quantum dots. For example, at a concentration of 30 μM of surface Cd atoms, no toxicity was observed from the silica coated quantum dots; while the bare quantum dots killed almost all the cells in a proliferation assay [83].

The second advantage of a silica coating is the improvement in surface properties of quantum dots. The surfaces of quantum dots are usually hydrophobic and difficult to functionalize. Modification by ligand exchange can provide quantum dots with greater hydrophilicity. Further surface functionalization, such as labeling with an antibody, is still a challenge using the ligand exchange method. In contrast, doping quantum dots inside silica nanoparticles not only significantly reduces the toxicities of quantum dots and improves their hydrophilicity, but also provides a convenient scaffold for further surface modification [71,104]. The silica surfaces can be easily functionalized by silica precursors, such as MPTS and APTS, to provide amine or thiol reactive groups. The functionalized surfaces can be further decorated with antibodies and proteins based on well-established chemical methods.

The unique luminescence properties of quantum dots are well-preserved or only slightly modified after being doped inside the silica matrix. In general, the excitation and emission spectra of the quantum dots remain the same. However, a decrease of luminescence quantum yield has been observed following the silica coating of quantum dots. One major reason is the change of local environment from organic ligands to the silica matrix. When a number of quantum dots are closely trapped inside a single silica nanoparticle, self-quenching also reduces their luminescence intensity. Hence, single-dot doped silica nanoparticles are preferred. Meanwhile, the synthetic conditions may be optimized to reduce photosystem changes to the coated quantum dots [97].

By the deliberate design of quantum dot doped silica nanoparticles, the nanohybrids inherit the advantages of both quantum dots and silica nanoparticles. Present applications of the hybrids are mainly related to bioimaging and biosensing. The silica-coated quantum dots can penetrate cell membranes via endocytosis [106]. Unlike those that are uncoated, silica-coated quantum dots cannot get through the nucleus membrane because of the expanded particle sizes. With proper outer-shell modification, quantum dot doped silica nanoparticles also can target the specific cells or specific sites on cells. For example, the membranes of cancer cells, HepG2 (human liver cancer cells) and 4T1 (mouse breast cancer cells), have been specifically labeled by the oleyl-modified quantum dot doped silica nanoparticles [93].

More recently, quantum dots are more likely to be doped in silica nanoparticles along with other dopants such as magnetic nanoparticles and magnetic resonance imaging (MRI) contrast agents. Such silica nanohybrids contain multiple components for tackling more realistic problems. Although quantum dot-silica nanohybrids have yet to reach maturity, their advantages and potential applications in the biological field have been amply demonstrated.

3.2. Magnetic nanoparticle nanohybrids

Magnetic nanoparticles have a great number of usages in medical treatments and for the separation of target molecules from a matrix. However, aggregation has been a problem for effective application of magnetic nanoparticles. The doping of magnetic nanoparticles into a silica matrix can successfully prevent magnetic nanoparticles from self-aggregation and from reacting with environmental species. As with quantum dot nanohybrids, the silica layer also serves as a medium for subsequent functionalization of the magnetic nanoparticles.

3.2.1. Synthesis

The formation of magnetic-silica nanohybrids can be divided into two categories. First, magnetic particles may be produced *in situ* in an amorphous silica matrix [108,109]. In this case, iron precursors are mixed with a silica gel or TEOS. A core–shell structure of the magnetic-silica nanohybrid is then formed through a calcination process [110–112] or by a flame spray pyrolysis approach [113]. This method allows for more magnetic nanoparticles to be incorporated in a single silica nanoparticle. However, the morphology of the resulting nanohybrids is uncontrollable.

The second method of synthesis is to prepare magnetite (Fe_3O_4) and maghemite (γ-Fe_2O_3) nanocrystals in advance through a co-deposition [114] or hydrothermal decomposition method [115]. After the nanocrystals form, a silica layer is post-coated on the nanocrystal surfaces. One of three methods may be used for the post-coating step: hydrolysis of silicate in acidic solutions, the Stöber method [111,116–118], or the reverse microemulsion method [119–122]. The first two methods fail to provide control over the size homogeneity of the nanoparticle. Several modified approaches have been developed to attain more uniform nanohybrids, as described below.

A thin silica layer can be initially formed on the bare magnetic particles using a small amount of silicate in order to change the isoelectric potential of the magnetic surface. Uniform nanohybrids can be obtained by growth of a silica shell on the stable colloids [123,124]. Similarly, magnetic nanoparticles can also be introduced into the system during the hydrolysis of TEOS. The previously formed SiO_2 particles can suppress the dipole–dipole interaction of the magnetic particles, thereby producing nanohybrids with defined shapes [125]. A sonication-assisted Stöber method can also provide dispersed magnetic nanoparticles while the hydrolysis of TEOS on magnetic cores is simultaneously stimulated. The hydrolysis can be completed in a short time period and, as a result, monodispersed silica-magnetic nanohybrids with a thin silica shell of a few nanometers can be obtained [126]. Other alternatives are a combination of miniemulsion–emulsion polymerization and sol–gel techniques [127] and a layer-by-layer method with the assistance of a polyelectrolyte [128] or polyvinylpyrrolidone [102].

With the reverse microemulsion method, the size of the nanohybrids can be easily controlled [129]. Both the magnetic crystal loading and the hybrid size can be tuned by changing the water to surfactant ratio or the TEOS concentration. Usually, a higher water to surfactant ratio yields smaller particles, whereas a higher TEOS concentration yields larger particles [130]. To avoid self-aggregation, magnetic nanoparticles are sometimes produced in a hydrophobic solution. In this case, it is essential to pre-treat the magnetic nanoparticles for successful transfer to an aqueous solution [131,132].

One additional shortcoming of the post-coating method is the limited number of magnetic nanoparticles that may be entrapped in a silica shell. To obtain a sufficient magnetic moment for recovery under an applied field, superparamagnetic clusters can be employed as core materials. These clusters are composed of numerous superparamagnetic nanocrystals normally prepared via the hydrothermal decomposition method [133]. Additionally, a sandwich of PVP-modified magnetic nanocrystals between two silica layers can avoid aggregation of magnetic nanocrystals and allow more nanocrystals to be loaded [102].

Recently, the development of mesoporous magnetic-silica nanohybrids has garnered attention because of their large adsorption capacities and facilitation of mass transfer [134]. In general, to make mesoporous nanohybrids, a surfactant (e.g. CTAB) is introduced into a suspension of magnetic particles with TEOS as the mesopore template. Surfactant molecules are trapped within the silica matrix during the hydrolysis process and, after the templates are removed by extraction with organic solvents or heat treatment, mesoporous structures are left behind [120,135]. Additionally, calcination of *n*-octadecyltrimethoxysilane-modified magnetic-silica nanohybrids also yields mesoporous structures, which are attributed to the existence of defects during the formation of the SiO_2 network [136].

3.2.2. Properties and applications

The behavior of magnetic nanoparticles is related to the thickness of their respective silica shells. Normally, a thicker silica shell reduces the inter-particle interaction and leads to superparamagnetism. It is also accompanied by a sacrifice in saturation magnetization (*Ms*) [137]. For instance, a 2 nm silica coating causes saturation magnetization to decrease from 90 emu/g for bare Fe_3O_4 nanoparticles to 60 emu/g [138]. Blocking temperature and particle size also affect the behavior of magnetic nanohybrids [139,140].

The applications of magnetic silica hybrids mainly fall into two categories. First of all, the nanohybrids may be used as enhancement agents for MRI, microwave-assisted protein digestion, and thermal therapy. MRI is a noninvasive diagnostic tool, capable of providing high spatial resolution images of tissues without using ionizing radiation. Since magnetic silica nanoparticles exhibit enhanced relaxivity and can hold a large number of active magnetic centers, the silica-magnetic nanohybrids show high potential to enhance MRI contrast [141]. Application of magnetic nanohybrids in microwave-assisted protein digestion takes advantage of the excellent microwave absorbability of magnetic particles. Trypsin-immobilized magnetic silica particles were designed for a microwave-assisted protein digestion purpose. Here, the microwaves absorbed by the magnetic particles greatly accelerated the reaction between enzyme (trypsin) and protein; thus, the incubation time was shortened to 15 s [142]. Finally, the fact that magnetic particles release heat under a magnetic field renders silica-magnetic nanohybrid as a promising thermal therapy agent.

The second application of magnetic silica hybrids is based on their field-induced transport for bioseparation [134,143], solid phase extraction, and catalyst removal [144–150]. The hybrids can be used to separate DNA, RNA and cells. At high salt concentrations, DNA strands can be adsorbed onto the magnetic-silica nanohybrids from a bacterial cell lysate [143,151]. Moreover, the magnetic silica hybrids have been successfully incorporated into the cells for easy cell removal from a solution by an external magnet [152]. This technique has advantages of greater speed and less contamination over traditional separation methods.

Magnetic-silica nanohybrids act as effective adsorbents to preconcentrate and separate analytes from the matrix. For instance, a nanohybrid was coated with a cationic lipid, didecyldimethylam-

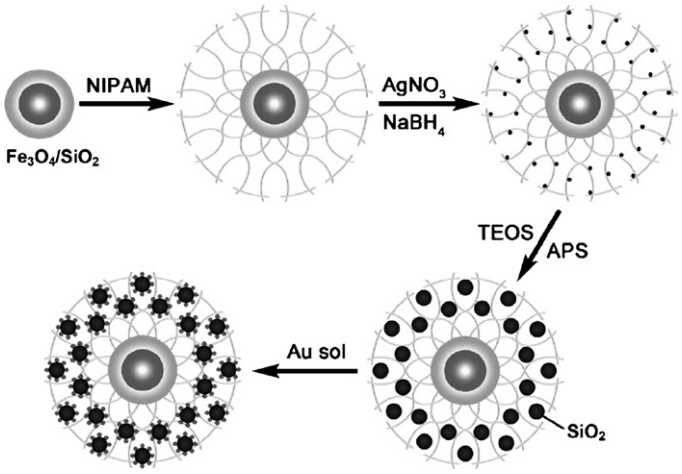

Scheme 5. Schematic illustration of the synthetic procedure from Fe_3O_4–SiO_2 colloids to $Fe_3O_4SiO_2$/p-NIPAM/SiO_2–Au assemblies. Reproduced with permission from Ref. [147].

monium bromide, to capture as few as 100 bacillus anthracis spores with 90% separation efficacy [149]. Additionally, the nanohybrids can remove metal ions, such as Cs^+, Sr^{2+}, and Co^{2+}, from the aqueous solution. The adsorption capacities were variable by changing pH since the surface charge of silica is pH-dependent [150].

Magnetic hybrids as carriers of catalysts offer advanced recovery of heterogeneous catalysts from reaction systems [110,119,144–146]. As shown in Scheme 5, a novel Au nanocatalyst was developed with a magnetic silica composite core and many small satellite silica sphere supports for the reduction of 4-nitrophenol. The catalyst was recovered magnetically while presenting a large reactive surface area [147]. Another heterogeneous catalyst was formed by growing polyaminoamido dendrons on magnetic-silica nanohybrids, which were then complexed with active metal components [144]. In addition to being coated on magnetic silica supports, catalysts can also be doped within a silica shell. Such a palladium-based separable catalyst was designed to catalyze multiple reactions [148]. In this case, although the silica shell could effectively protect the catalytic activity, it created difficulties for the reactants to effectively reach the catalysts.

Even at this early stage of their development, magnetic-silica nanohybrids have found a broad range of applications. The latest developments with magnetic nanohybrids have trended toward materials with multiple functionalities. A typical example is the recently developed nanohybrid that combined the functions of drug delivery, magnetic resonance imaging, fluorescence imaging and identification of target cancer cells [153]. Although magnetic separation has been the most traditional end-use for these materials and will continue to be so, it is also clear that these nanohybrids can provide a wider scope of use and may find other applications outside the bounds of separation.

3.3. Gold nanomaterial nanohybrids

Gold nanomaterials are typically photoactive. The synthesis and surface modification of gold nanomaterials have been well documented [154–156]. In addition to functioning as individual photosensitive probes, gold nanomaterials are often used to enhance detection signals, such as metal-enhanced fluorescence, fluorescence resonance energy transfer and surface enhanced Raman scattering (SERS). Occasionally, gold nanomaterials are also used for photothermal therapy [157–161]. The principles of metal enhanced fluorescence and SERS have been well studied [162]. Gold and silver are the most commonly used metals for enhancement. Silver exhibits a much higher enhancement than gold but a lower stability. In this section, gold nanomaterials are discussed.

Silica nanomaterials can adjust the optical properties of gold nanomaterials when the hybrid is formed. The shape, size and structure of both silica and gold affect the property of the hybrids. In fact, the gold–silica nanohybrids may be built into various configurations for different applications. For instance, hybrids with a silica core and a gold shell exhibit an extinction peak in the NIR region. In the opposite configuration – a gold core with a silica shell – the hybrid exhibits an extinction peak in the visible region [163]. Due to these highly variable properties, the gold–silica nanohybrids have gained considerable attention. The works covered in this section are synthesis, properties and initial applications of the gold–silica nanohybrids. It is expected that a wider range of applications will be developed with these hybrids in the near future.

3.3.1. Synthesis

The approach of doping gold nanomaterials into the silica matrix consists of a few sequential steps: synthesis of gold cores, stabilization of the core, and formation of the coating layer of silica onto the gold core [164,165]. The gold nanoparticle core is usually synthesized via the traditional chemical method [163]. The stabilization of the gold core can be conducted using a polymer, PVP, which can attach to both silica and gold surfaces and initiate the growth of silica on the gold surface [166]. To achieve a homogeneous and monodispersed silica coating layer, PVP of different molecular weights (mw) are required to coat gold nanoparticles of different sizes. For example, PVP10 (mw = 10,000) is suitable to treat small gold nanoparticles (e.g. 15 nm in diameter), and PVP40 (mw = 40,000) is preferred for the large gold nanoparticles (e.g. 250 nm in diameter) [166]. When the positively charged surfactant CTAB is used to stabilize gold nanorods, it can directly attract the negatively charged silica precursor TEOS. As a result, mesoporous silica shells form on the gold nanorods [103].

The affinity between the gold and silica is weaker than those between quantum dots or magnetic nanoparticles and silica. An anchor precursor such as MPTS or APTS is required for the surface-targeted growth of silica [167,168]. Then, the hydrolysis of TEOS through either the Stöber method or the reverse microemulsion method forms a second silica layer. To coat a dense silica shell, a layer-by-layer deposition of polyelectrolytes, polystyrene sulfate and poly(allylamine hydrochloride) (PAH), may be applied [58,169]. After CTAB is blocked by layers of polyelectrolytes, a dense silica shell starts growing on the positively charged PAH modified gold nanorod surface. Instead of Stöber or reverse microemulsion methods, gold–silica core–shell nanoparticle can be prepared in a "reverse" synthesis [170]. In this method, hollow silica nanoparticles are first synthesized, followed by an *in situ* growth of gold core inside the hollow silica shell.

The variable structures of the hybrids provide different enhancements in the application of gold–silica nanohybrids to SERS or metal-enhanced fluorescence. A special structure of silica–void–gold hybrid was developed for SERS (Fig. 6) [171]. Sodium hydroxide was used to etch the silica. A prolonged etching time resulted in a much thinner shell of silica with numerous open channels.

The fabrication of silica–gold core–shell nanohybrid usually requires a silica nanoparticle with an amine-enriched surface as the core [172–174]. The formation of a gold shell on this core is based on a gold seed growth method (Fig. 7) [163]. First, gold seeds are immobilized on silica surface through an amine bond [174]. The binding efficiency is greatly affected by the reaction pH [175]. In basic conditions, the amine groups are prone to bond to gold seeds. While in an acidic environment, the protonated amine groups are less effective for gold seed binding. After the seeds are attached on the silica surface, their further growth leads to the formation of a

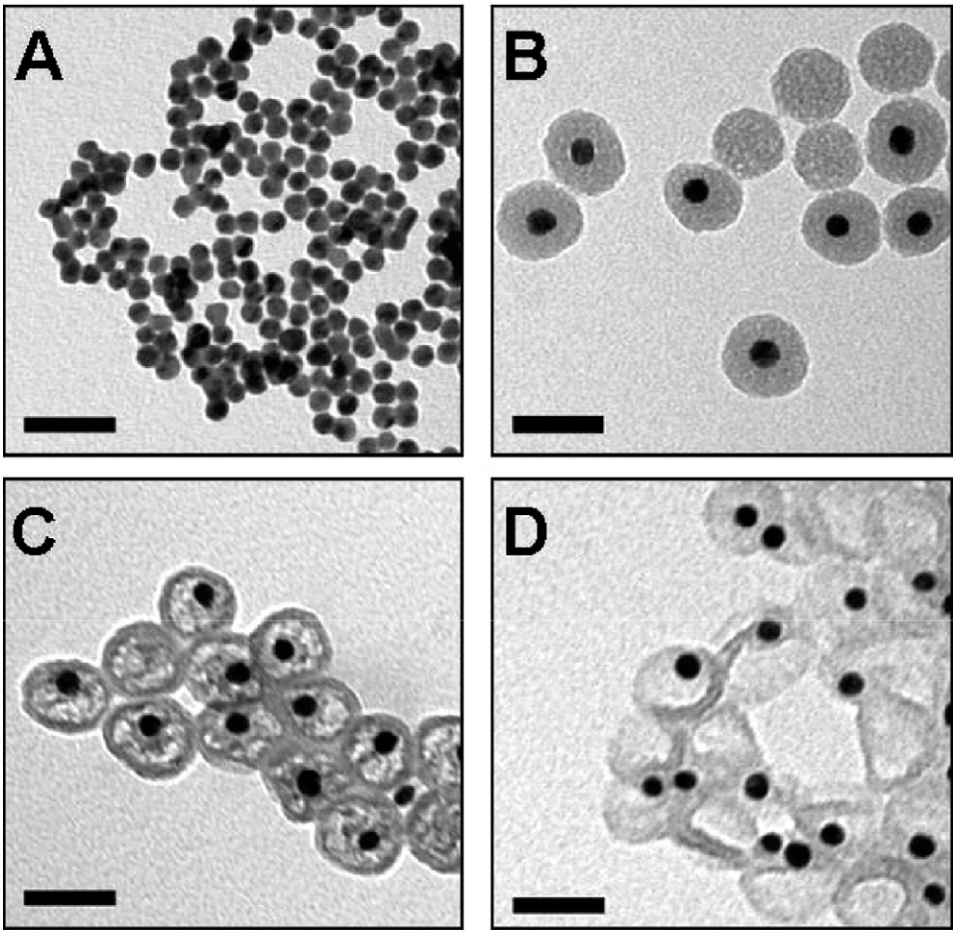

Fig. 6. Gold–void–silica nanohybrids. (A and B) TEM images of gold nanoparticles and gold–silica nanohybrid. (C and D) TEM images of gold–void–silica nanohybrids. Scale bar: 50 nm. Reproduced with permission from Ref. [171].

gold shell. The thickness of gold shell can be adjusted by changing the amount of the growth reagent, chloroauric acid ($HAuCl_4$) [157,176].

3.3.2. Properties and applications

One exceptional property of gold nanomaterials is their tunable extinction spectra by varying their sizes and shapes, or the inner and outer diameters of the gold shell [157,158,177]. As the shape of the gold nanomaterial changes from a sphere to a rod, its extinction peak shifts from 500 nm to the NIR region [155]. The absorption peak of a silica–gold nanohybrid moves towards longer wavelengths as the inner cavity becomes larger [157,158]. The aggregation of gold nanoparticles causes a red-shift in the gold spectrum [163].

The main applications of gold–silica nanohybrids are in the areas of optical sensing and labeling. However, the nanohybrid-enhanced NIR emission is particularly useful for the photothermic therapy due to the deep penetration of NIR irradiation into living systems [178–180]. A typical photothermic therapy process starts with the surface immobilization of an antibody against a tumor cell, such as vicinal malignant cells. The antibody then directs nanohybrid binding to tumor cells within a living system. The hybrid absorbs the energy from the NIR irradiation, generating heat to kill the target cell [178,179]. An *in vivo* study with mice showed that such a

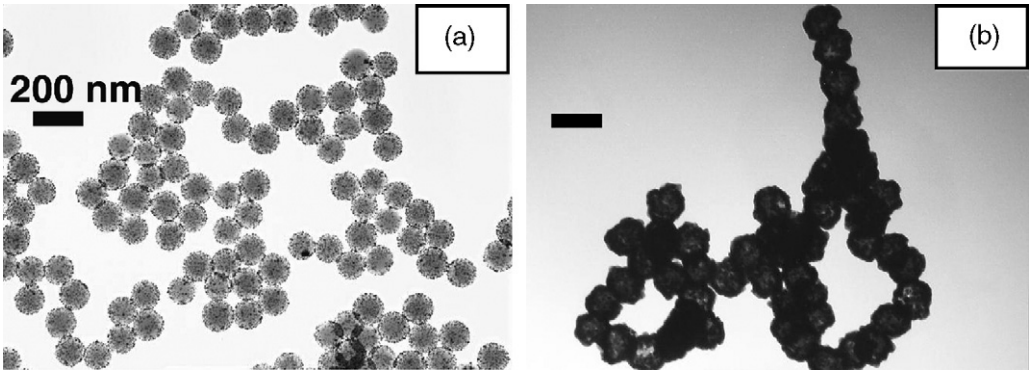

Fig. 7. TEM images of (A) gold seed coated silica nanoparticles and (B) silica–gold core–shell nanoparticles. Reproduced with permission from Ref. [163].

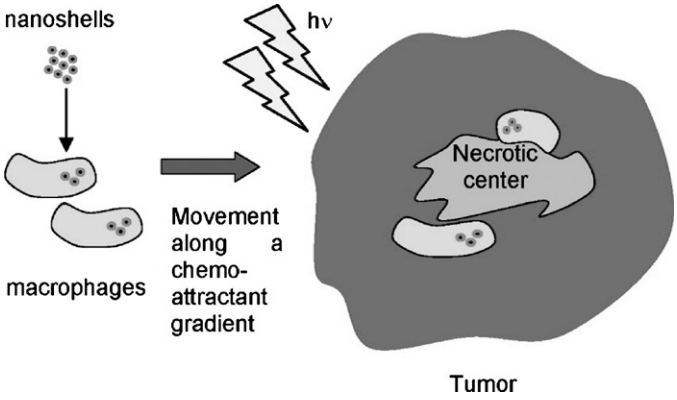

Scheme 6. Delivery of the nanohybrids to tumor site via monocytes. Reproduced with permission from Ref. [180].

treatment significantly reduced the tumor size and increased the frequency of survival [179]. Instead of the antibody-oriented delivery, the gold–silica nanohybrids can also target the tumor region via monocytes. The nanohybrids first penetrate into the manocytes which are then enriched by a malignant neoplasm (Scheme 6) [180].

The enhancement of molecular fluorescence by gold nanomaterials, a property which provides significant advantages for sensing and detection applications, requires two conditions: a suitable distance between the dye and the metal surface (10–100 nm), and overlapping wavelengths of the gold nanomaterial absorption peak and the excitation or emission peak of dye molecules [162,181–184]. To meet these two requirements, a nanohybrid can be designed by appropriately assembling the gold nanomaterials along with the dye molecules into a silica nanoparticle matrix. Both the distance and the gold absorption peak are adjustable in the design. Thus, the gold-fluorescent silica nanohybrids are an effective unit for fluorescence enhancement.

The silica shell can prevent the aggregation of gold nanomaterials for reproducible and stable SERS signals. However, SERS requires the direct contact of the analyte with metal surfaces. So far, the application of the gold–silica hybrid in SERS is limited. A special gold–void–silica structure can provide appropriate space for the direct contact in SERS [171].

In summary, gold–silica nanohybrids have advanced the applications of pure gold nanomaterials. The assembly of functional components along with gold nanomaterials in a silica matrix provides nanohybrids with multiple functions. The structure of the hybrids can be designed for different applications.

3.4. Catalytic nanohybrids

Amorphous silica constitutes a novel type of catalyst support because of its porous structure, high thermal stability, optical transparency and chemical inertness. Initial research results have demonstrated that the silica supports can enhance catalyst stability, reactivity and selectivity. Although this is a relatively new area, the immobilization of catalysts onto silica supports has received considerable attention. In this section, two types of silica–catalyst hybrids are covered with an emphasis on silica–titania hybrids.

3.4.1. Silica-based metal catalysts

The uniform distribution of catalysts on silica surfaces is a challenge. Initially, silica nanoparticles are first suspended in a metal salt solution. The metal salt as a precursor is physically adsorbed onto the silica surface where it is reduced to a metal nanoparticle. However, the early-forming metal nanoparticles tend to induce the deposition of more metal crystals onto the same silica nanoparticle, resulting in the formation of large metal aggregates [185].

To solve this problem, stronger interactions between the silica support and the metal precursor are recommended should be stronger than simple electrostatics. Both covalent bonds [186–188] and H-bond [189,190] have been effectively employed. A metal-template/metal-exchange method was developed based on a covalent bond between Mn(II) and silica. The resulting catalyst hybrid showed an enhanced reactivity and selectivity compared to the randomly grafted analogue [191]. Usually, organometallic complexes containing sulfonate groups can directly link to the silica support based on the strong H-bond between sulfonate groups and terminal silanols of silica. Finally, a monolayer of catalyst is formed on the silica supports. Another approach aiming to control size distribution of metal catalysts is to encapsulate pre-synthesized metal nanocrystals within mesoporous silica supports via sonication or supercritical CO_2 [192–194]. The catalyst loading can be controlled by tuning the force between the solvent and CO_2 [195].

3.4.2. Silica-based titania nanohybrids

Titania is one of the most commonly used semiconductor photocatalysts due to its low cost, low toxicity and high chemical resistance. Photoelectrons are excited while the titania is exposed to UV radiation. The generated electron–hole pairs serve as reducing and oxidizing agents for various redox reactions. One of the broad applications of titania is to address environmental pollution, including degradation of air pollutants (i.e., nitrogen oxides, aromatics, chlorofluorocarbons, mustard gas [196,197], mercury [198]), water purification [199] and photomineralization of various organic pollutants (i.e., aromatics [200], dyes [201], and pesticides). Silica–titania nanohybrids are now emerging photocatalysts. The silica supports not only increase the thermal stability and dispersion of titania, but also enhance the catalytic activity of titania.

3.4.2.1. Synthesis. The synthesis of silica-supported titania usually starts at the dispersion of silica nanoparticles in an absolute organic solvent (i.e., ethyl alcohol [202] or toluene [203]) to prevent the rapid and uncontrollable hydrolysis of Ti precursors. A small amount of water is then introduced into the solution before the addition of Ti precursors. The water layer on the silica surface serves as a nanoreactor for hydrolysis and condensation of titanium precursors [202]. Other methods to synthesize silica–titania nanohybrids include microemulsion [204–207], impregnation, precipitation, chemical vapor deposition [208,209] and sol–gel methods [210,211]. These methods usually produce core–shell nanohybrids with a uniform thin titania outer layer. If a large titania loading is required (>30%), a multistep coating is recommended [212].

3.4.2.2. Properties and applications. The photocatalytic activity of titania depends upon its crystallinity, particle size and crystal phase. Titania has three major crystal forms: anatase, rutile and brookie. Among them, anatase is a kinetically stable phase and gives the highest catalytic activity. The rutile phase is a thermally stable form and usually emerges from conversion of anatase at elevated temperatures. Studies have revealed that the presence of a silica component can enhance the thermal stability of anatase phase and effectively prevent the growth of titania particle sizes [213]. The formation of the Ti–O–Si bond inhibits the changes of the O–Ti–O bond angle and the O–O distance, which are required for the phase transition [214]. As a result, the presence of silica supports increases the temperature of anatase-to-rutile phase transformation from 450 °C to 900 °C [200].

SiO_2 supports increase the acidity of TiOH and thus increase the catalytic activity of titania [203,215]. The Ti–O–Si bonds at the interface of silica and titania decrease the electron mobility of titania. It has been revealed that the silica supports result in a significant anodic shift of both the conduction and valence bands of titania,

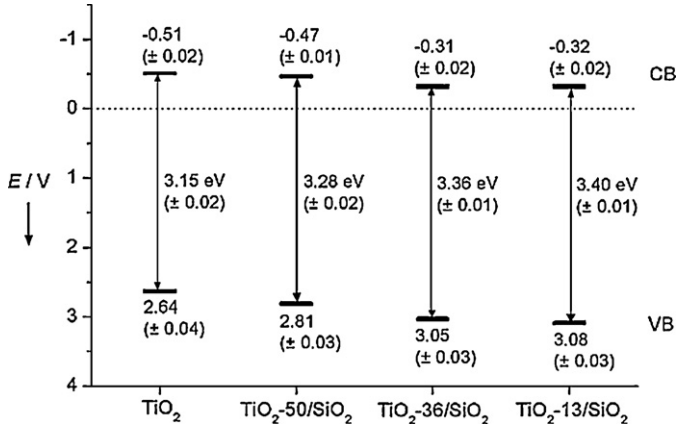

Fig. 8. Bandgap energies and band-edge positions (pH 7) for different SiO_2–TiO_2 materials. The values for valence band (VB) and conduction band edges (CB) are given in volts (vs. NHE). Reproduced with permission from Ref. [217].

accompanied with the widen bandgap (Fig. 8) [216,217]. Although this effect decreases the reducing ability of titania [217], its oxidizing activity is increased significantly.

Silica matrices inhibit the electron–hole recombination on titania surfaces. In the study of water splitting reaction catalyzed by the SiO_2–TiO_2 nanohybrids, the presence of silica significantly increased photocurrent and photovoltaic efficiency. The silica layer creates an energy barrier that suppresses the recombination of electrons with holes at the interface of titania and electrolytes [218,219].

Ti loading on silica supports impacts catalytic activity. At a low Ti loading, the titanium species tend to prefer tetrahedral coordination at the interface of titania and silica. The maximum titanium coverage can reach ~2.2 Ti atom/nm^2. With the increase of Ti loading, more octahedral Ti-sites are prone to anchoring on the silica. The catalytic activity reaches its maximum when a titania monolayer is formed since tetrahedral Ti species are the most active [220,221].

The type of titanium precursor also affects the photocatalytic properties of the titania–silica hybrids. Hybrids produced by $Ti(SO_4)_2$ exhibit higher photocatalytic activity than those synthesized from $TiCl_3$. The sulfate ion of $Ti(SO_4)_2$ might generate both acidic and photoactive sites on titania surface and the increased acidity is believed to promote the photocatalytic activity [222,223].

A shortcoming of native titania photocatalysts is their limited spectral absorption which comprises only UV wavelengths and only amounts to 30% of available solar energy. To more efficiently utilize available solar energy, certain transition metal ions (e.g. Cr^{6+}, Co^{3+}) have been doped into the titania–silica nanohybrids in order to shift the excitation wavelength of the modified titania from the UV and toward the visible region [224].

Overall, silica–titania nanohybrids have demonstrated an obvious enhancement of titania photoactivity. The improved photocatalytic performance is attributed to the increased surface area, surface acidity, local concentration of adsorbed reactants, and suppressed electron–hole recombination [99,214]. The need for highly effective and inexpensive catalysts will drive a rapid development of titania–silica hybrids in the near future.

4. Conclusions

In summary, amorphous silica nanoparticles are an excellent matrix for hybridization with functional molecules and nanomaterials. Commonly used fluorescent molecules and drugs can be doped inside the silica nanomatrix. The resultant nanohybrids exhibit enhanced abilities over the pure molecules. Commercially available functional nanomaterials including quantum dots, gold nanomaterials, magnetic nanoparticles and nanocatalysts, can also form nanohybrids with a silica matrix. These nanohybrids generally share the advantageous properties of both silica and the functional nanomaterials. The synthesis of the silica nanohybrids has been well studied and a variety of applications of these nanohybrids has been demonstrated. The future development of the silica nanohybrids will likely be focused on various multiple-functional hybrids for solving practical problems. For example, nanohybrids that combine the functions of diagnosis, drug delivery and therapy will be efficient and promising nanomaterials for biomedical studies.

Acknowledgments

The work was supported by the National Science Foundation under grant CHE-0616878 and REU grant CHE -0552762, the U.S. Department of Energy under grant DE-FG02-6ER46292), a University of North Dakota Doctoral Dissertation Assistantship and North Dakota Water Resource Research Institute Graduate Student Assistantship, and seed awards from the North Dakota EPSCoR. Neither the United States Government nor the agency thereof, nor any of the employees, makes any warranty, express or implied, or assumes any legal liability or responsibility for the accuracy, completeness, or usefulness of any information disclosed. Reference herein does not necessarily constitute or imply its endorsement, recommendation, or favoring by the United States Government or the agency thereof or by the State of North Dakota.

References

[1] A. Burns, H. Ow, U. Wiesner, Chem. Soc. Rev. 35 (2006) 1028.
[2] W. Tan, K. Wang, X. He, X.J. Zhao, T. Drake, L. Wang, R.P. Bagwe, Med. Res. Rev. 24 (2004) 621.
[3] L. Wang, K. Wang, S. Santra, X. Zhao, L.R. Hilliard, J. Smith, Y. Wu, W. Tan, Anal. Chem. A 78 (2006) 646.
[4] X. Zhao, L.R. Hilliard, K. Wang, W. Tan, in: H.S. Nalwa (Ed.), Encyclopedia of Nanoscience and Nanotechnology, American Scientific Publishers, Stevenson Ranch, 2004, p. 255.
[5] G. Yao, L. Wang, Y. Wu, J. Smith, J.Z. Xu, E.W. Lee, W. Tan, Anal. Bioanal. Chem. 385 (2006) 518.
[6] W. Stöber, A. Fink, J. Colloid Interface Sci. 26 (1968) 62.
[7] H. Ow, D. Larson, M. Srivastava, B. Baird, W. Webb, U. Wiesner, Nano Lett. 5 (2005) 113.
[8] L. Wang, W. Tan, Nano Lett. 6 (2006) 84.
[9] Y. Jin, S. Lohstreter, D.T. Pierce, J. Parisien, M. Wu, C. Hall III, X. Zhao, Chem. Mater. 20 (2008) 4411.
[10] F. Arriagada, K. Osseo-Asare, Colloids Surf. 154 (1999) 311.
[11] R.P. Bagwe, C. Yang, L.R. Hilliard, W. Tan, Langmuir 20 (2004) 8336.
[12] L. Wang, C. Yang, W. Tan, Nano Lett. 5 (2005) 37.
[13] X. Zhao, R.P. Bagwe, W. Tan, Adv. Mater. 16 (2004) 173.
[14] S. Santra, H. Yang, D. Dutta, J.T. Stanley, P.H. Holloway, W. Tan, B.M. Moudgil, R.A. Mericle, Chem. Commun. 24 (2004) 2810.
[15] M. Montalti, L. Prodi, N. Zaccheroni, G. Falini, J. Am. Chem. Soc. 124 (2002) 13540.
[16] S. Bonacchi, E. Rampazzo, M. Montalti, L. Prodi, N. Zaccheroni, F. Mancin, P. Teolato, Langmuir 24 (2008) 8387.
[17] D. Gao, Z. Wang, B. Liu, L. Ni, M. Wu, Z. Zhang, Anal. Chem. 80 (2008) 8545.
[18] E. Rampazzo, E. Brasola, S. Marcuz, F. Mancin, P. Tecilla, U. Tonellato, J. Mater. Chem. 15 (2005) 2687.
[19] M. Montalti, L. Prodi, N. Zaccheroni, G. Battistini, S. Marcuz, F. Mancin, E. Rampazzo, U. Tonellato, Langmuir 22 (2006) 5877.
[20] E. Rampazzo, S. Bonacchi, M. Montalti, L. Prodi, N. Zaccheroni, J. Am. Chem. Soc. 129 (2007) 14251.
[21] X. Zhao, L.R. Hilliard, S.J. Mechery, Y. Wang, R.P. Bagwe, S. Jin, W. Tan, Proc. Natl. Acad. Sci. U.S.A. 101 (2004) 15027.
[22] L. Wang, W. Zhao, M.B. O'Donoghue, W. Tan, Bioconjug. Chem. 18 (2007) 297.
[23] J.E. Smith, C.D. Medley, Z. Tang, D. Shangguan, C. Lofton, W. Tan, Anal. Chem. 79 (2007) 3075.
[24] X. Zhao, R. Tapec-Dytioco, W. Tan, J. Am. Chem. Soc. 125 (2003) 11474.
[25] A. Burns, P. Sengupta, T. Zedayko, B. Baird, U. Wiesner, Small 2 (2006) 723.
[26] S.M. Buck, Y.L. Koo, E. Park, H. Xu, M.A. Philbert, M.A. Brasuel, R. Kopelman, Curr. Opin. Chem. Biol. 8 (2004) 540.
[27] H. Xu, J.W. Aylott, R. Kopelman, T.J. Miller, M.A. Philbert, Anal. Chem. 73 (2001) 4124.
[28] Y.L. Koo, Y. Cao, R. Kopelman, S.M. Koo, M. Brasuel, M.A. Philbert, Anal. Chem. 76 (2004) 2498.
[29] M. Arduini, F. Mancin, P. Tecilla, U. Tonellato, Langmuir 23 (2007) 8632.

[30] S.H. Kim, M. Jeyakumar, J.A. Katzenellenbogen, J. Am. Chem. Soc. 129 (2007) 13254.
[31] W. Miao, J.P. Choi, A.J. Bard, J. Am. Chem. Soc. 124 (2002) 14478.
[32] C.A. Marquette, L.J. Blum, Anal. Bioanal. Chem. 385 (2006) 546.
[33] L. Qian, X. Yang, Adv. Funct. Mater. 17 (2007) 1353.
[34] L. Zhang, S. Dong, Anal. Chem. 78 (2006) 5119.
[35] L. Zhang, S. Dong, Electrochem. Commun. 8 (2006) 1687.
[36] L. Zhang, F. Wang, S. Dong, Electrochim. Acta 53 (2008) 6423.
[37] X. Hun, Z. Zhang, Sens. Actuators B 131 (2008) 403.
[38] X. Hun, Z. Zhang, J. Pharmaceut. Biomed. 47 (2008) 670.
[39] X. Wang, J. Zhou, W. Yun, S. Xiao, Z. Chang, P. He, Y. Fang, Anal. Chim. Acta 598 (2007) 242.
[40] Z. Chang, J. Zhou, K. Zhao, N. Zhu, P. He, Y. Fang, Electrochim. Acta 52 (2006) 575.
[41] K. Qian, L. Zhang, M. Yang, P. He, Y. Fang, Chinese J. Chem. 22 (2004) 702.
[42] L. Zhang, X. Zheng, Anal. Chim. Acta 570 (2006) 207.
[43] L. Zhang, X. Zheng, Z. Guo, Chinese J. Chem. 25 (2007) 351.
[44] H. Wei, J. Liu, L. Zhou, J. Li, X. Jiang, J. Kang, X. Yang, S. Dong, E. Wang, Chem. Eur. J. 14 (2008) 3687.
[45] S. Kim, T.Y. Ohulchanskyy, H.E. Pudavar, R.K. Pandey, P.N. Prasad, J. Am. Chem. Soc. 129 (2007) 2669.
[46] W. Tang, H. Xu, R. Kopelman, M.A. Philbert, Photochem. Photobiol. 81 (2005) 242.
[47] D.J. Bharali, I. Klejbor, E.K. Stachowiak, P. Dutta, I. Roy, N. Kaur, E.J. Bergey, P.N. Prasad, M.K. Stachowiak, Proc. Natl. Acad. Sci. U.S.A. 102 (2005) 11539.
[48] T.Y. Ohulchanskyy, I. Roy, L.N. Goswami, Y. Chen, E.J. Bergey, R.K. Pandey, A.R. Oseroff, P.N. Prasad, Nano Lett. 7 (2007) 2835.
[49] I. Roy, T.Y. Ohulchanskyy, D.J. Bharali, H.E. Pudavar, R.A. Mistretta, N. Kaur, P.N. Prasad, Proc. Natl. Acad. Sci. U.S.A. 102 (2005) 279.
[50] B. Thierry, L. Zimmer, S. McNiven, K. Finnie, C. Barbé, H.J. Griesser, Langmuir 24 (2008) 8143.
[51] M.M. van Schooneveld, E. Vucic, R. Koole, Y. Zhou, J. Stocks, D.P. Cormode, C.Y. Tang, R.E. Gordon, K. Nicolay, A. Meijerink, Z.A. Fayad, W.J.M. Mulder, Nano Lett. 8 (2008) 2517.
[52] F. Caruso, R.A. Caruso, H. Mohwald, Science 282 (1998) 1111.
[53] Z. Li, L. Wen, L. Shao, J. Chen, J. Control Release 98 (2004) 245.
[54] J. Yang, J. Lee, J. Kang, K. Lee, J. Suh, H. Yoon, Y. Huh, S. Haam, Langmuir 24 (2008) 3417.
[55] Y. Liu, H. Miyoshi, M. Nakamura, Colloids Surf. B: Biointerfaces 58 (2007) 180.
[56] F. Caruso, Chem. Eur. J. 6 (2000) 413.
[57] J. Chen, H. Ding, J. Wang, L. Shao, Biomaterials 25 (2004) 723.
[58] I. Pastoriza-Santos, J. Prez-Juste, L.M. Liz-Marzn, Chem. Mater. 18 (2006) 2465.
[59] Q. Zhang, T. Zhang, J. Ge, Y. Yin, Nano Lett. 8 (2008) 2867.
[60] T. Zhang, J. Ge, Y. Hu, Q. Zhang, S. Aloni, Y. Yin, Angew. Chem. Int. Ed. 47 (2008) 5806.
[61] J.A. Phillips, D. Lopez-Colon, Z. Zhu, Y. Xu, W. Tan, Anal. Chim. Acta 621 (2008) 101.
[62] D. Luo, W.M. Saltzman, Gene Ther. 13 (2006) 585.
[63] E.W. Choi, H.C. Koo, S.I. Shin, Y.J. Chae, J.H. Lee, S.M. Han, S.J. Lee, D.H. Bhang, Y.H. Park, C.W. Lee, H.Y. Youn, Exp. Hematol. 36 (2008) 1091.
[64] D. Luo, E. Han, N. Belcheva, W.M. Saltzman, J. Control Release 95 (2004) 333.
[65] L.M. Rossi, P.R. Silva, L.L.R. Vono, A.U. Fernandes, D.B. Tada, M.S. Baptista, Langmuir 24 (2008) 12534.
[66] F. Yan, R. Kopelman, Photochem. Photobiol. 78 (2003) 587.
[67] Z.A. Peng, X. Peng, J. Am. Chem. Soc. 123 (2001) 183.
[68] C.B. Murray, D.J. Norris, M.G. Bawendi, J. Am. Chem. Soc. 115 (1993) 8706.
[69] B.A. Kairdolf, A.M. Smith, S. Nie, J. Am. Chem. Soc. 130 (2008) 12866.
[70] W.C.W. Chan, S. Nie, Science 281 (1998) 2016.
[71] M.P. Bruchez, M. Moronne, P. Gin, S. Weiss, A.P. Alivisatos, Science 281 (1998) 2013.
[72] A.P. Alivisatos, Science 271 (1996) 933.
[73] X. Wu, H. Liu, J. Liu, K.N. Haley, J.A. Treadway, J.P. Larson, N. Ge, F. Peale, M.P. Bruchez, Nat. Biotechnol. 21 (2003) 41.
[74] A.M. Smith, H. Duan, A.M. Mohs, S. Nie, Adv. Drug Deliv. Rev. 60 (2008) 1226.
[75] X. Michalet, F.F. Pinaud, L.A. Bentolila, J.M. Tsay, S. Doose, J.J. Li, G. Sundaresan, A.M. Wu, S.S. Gambhir, S. Weiss, Science 307 (2005) 538.
[76] I.L. Medintz, H.T. Uyeda, E.R. Goldman, H. Mattoussi, Nat. Mater. 4 (2005) 435.
[77] R. Gill, M. Zayats, I. Willner, Angew. Chem. Int. Ed. 47 (2008) 7602.
[78] X. Gao, Y. Cui, R.M. Levenson, L.W.K. Chung, S. Nie, Nat. Biotechnol. 22 (2004) 969.
[79] B. Dubertret, P. Skourides, D.J. Norris, V. Noireaux, A.H. Brivanlou, A. Libchaber, Science 298 (2002) 1759.
[80] A. Shiohara, A. Hoshino, K. Hanaki, K. Suzuki, K. Yamamoto, Microbiol. Immunol. 48 (2004) 669.
[81] A. Nel, T. Xia, L. Mädler, N. Li, Science 311 (2006) 622.
[82] J. Lovric, H.S. Bazzi, Y. Cuie, G.R. Fortin, F.M. Winnik, D. Maysinger, J. Mol. Med. 83 (2005) 377.
[83] C. Kirchner, T. Liedl, S. Kudera, T. Pellegrino, J.A. Munoz, H.E. Gaub, S. Stolzle, N. Fertig, W.J. Parak, Nano Lett. 5 (2005) 331.
[84] A. Hoshino, K. Fujioka, T. Oku, M. Suga, Y.F. Sasaki, T. Ohta, M. Yasuhara, K. Suzuki, K. Yamamoto, Nano Lett. 4 (2004) 2163.
[85] R. Hardman, Environ. Health Perspect. 114 (2006) 165.
[86] M. Green, E. Howman, Chem. Commun. (2005) 121.
[87] A.M. Derfus, W.C.W. Chan, S.N. Bhatia, Nano Lett. 4 (2004) 11.
[88] W. Chan, N. Shiao, P. Lu, Toxicol. Lett. 167 (2006) 191.
[89] D.K. Yi, S.T. Selvan, S.S. Lee, G.C. Papaefthymiou, D. Kundaliya, J.Y. Ying, J. Am. Chem. Soc. 127 (2005) 4990.
[90] Y. Yang, M. Gao, Adv. Mater. 17 (2005) 2354.
[91] T.T. Tan, S.T. Selvan, L. Zhao, S. Gao, J.Y. Ying, Chem. Mater. 19 (2007) 3112.
[92] S.T. Selvan, T.T. Tan, J.Y. Ying, Adv. Mater. 17 (2005) 1620.
[93] S.T. Selvan, P.K. Patra, C.Y. Ang, J.Y. Ying, Angew. Chem. Int. Ed. 46 (2007) 2448.
[94] W. Law, K. Yong, I. Roy, G. Xu, H. Ding, E.J. Bergey, H. Zeng, P.N. Prasad, J. Phys. Chem. C 112 (2008) 7972.
[95] R. Koole, M.M. van Schooneveld, J. Hilhorst, C. de Mello Donegá, D.C. 't Hart, A. van Blaaderen, D. Vanmaekelbergh, A. Meijerink, Chem. Mater. 20 (2008) 2503.
[96] M. Darbandi, R. Thomann, T. Nann, Chem. Mater. 17 (2005) 5720.
[97] Z. Zhelev, H. Ohba, R. Bakalova, J. Am. Chem. Soc. 128 (2006) 6324.
[98] T. Zhang, J.L. Stilwell, D. Gerion, L. Ding, O. Elboudwarej, P.A. Cooke, J.W. Gray, A.P. Alivisatos, F.F. Chen, Nano Lett. 6 (2006) 800.
[99] A. Wolcott, D. Gerion, M. Visconte, J. Sun, A. Schwartzberg, S. Chen, J.Z. Zhang, J. Phys. Chem. B 110 (2006) 5779.
[100] T. Nann, P. Mulvaney, Angew. Chem. Int. Ed. 43 (2004) 5393.
[101] N. Insin, J.B. Tracy, H. Lee, J.P. Zimmer, R.M. Westervelt, M.G. Bawendi, ACS Nano. 2 (2008) 197.
[102] C. Graf, S. Dembski, A. Hofmann, E. Rhl, Langmuir 22 (2006) 5604.
[103] I. Gorelikov, N. Matsuura, Nano Lett. 8 (2008) 369.
[104] D. Gerion, F. Pinaud, S.C. Williams, W.J. Parak, D. Zanchet, S. Weiss, A.P. Alivisatos, J. Phys. Chem. B 105 (2001) 8861.
[105] R. Bakalova, Z. Zhelev, I. Aoki, H. Ohba, Y. Imai, I. Kanno, Anal. Chem. 78 (2006) 5925.
[106] R. Bakalova, Z. Zhelev, I. Aoki, K. Masamoto, M. Mileva, T. Obata, M. Higuchi, V. Gadjeva, I. Kanno, Bioconjug. Chem. 19 (2008) 1135.
[107] Y. Jin, S. Kannan, M. Wu, J.X. Zhao, Chem. Res. Toxicol. 20 (2007) 1126.
[108] S.-H. Hu, T.-Y. Liu, H.-Y. Huang, D.-M. Liu, S.-Y. Chen, Langmuir 24 (2008) 239.
[109] R.Y. Hong, H.P. Fu, G.Q. Di, Y. Zheng, D.G. Wei, Mater. Chem. Phys. 108 (2008) 132.
[110] A. Nomura, S. Shin, O.O. Mehdi, J.-M. Kauffmann, Anal. Chem. 76 (2004) 5498.
[111] G. Ennas, A. Falqui, S. Marras, C. Sangregorio, G. Marongiu, Chem. Mater. 16 (2004) 5659.
[112] Y. Kobayashi, M. Horie, M. Konno, B. Rodriguez-Gonzalez, L.M. Liz-Marzan, J. Phys. Chem. B 107 (2003) 7420.
[113] D. Li, W.Y. Teoh, C. Selomulya, R.C. Woodward, R. Amal, B. Rosche, Chem. Mater. 18 (2006) 6403.
[114] S. Santra, R. Tapec, N. Theodoropoulou, J. Dobson, A. Hebard, W. Tan, Langmuir 17 (2001) 2900.
[115] S. Sun, H. Zeng, J. Am. Chem. Soc. 124 (2002) 8204.
[116] D. Ma, J. Guan, S. Denommee, G. Enright, T. Veres, B. Simard, Chem. Mater. 18 (2006) 1920.
[117] M.F. Casula, A. Corrias, A. Falqui, V. Serin, D. Gatteschi, C. Sangregorio, C. de Julian Fernandez, G. Battaglin, Chem. Mater. 15 (2003) 2201.
[118] Y. Lu, Y. Yin, B.T. Mayers, Y. Xia, Nano Lett. 2 (2002) 183.
[119] S.C. Tsang, C.H. Yu, X. Gao, K. Tam, J. Phys. Chem. B 110 (2006) 16914.
[120] Y.-S. Lin, S.-H. Wu, Y. Hung, Y.-H. Chou, C. Chang, M.-L. Lin, C.-P. Tsai, C.-Y. Mou, Chem. Mater. 18 (2006) 5170.
[121] C.R. Vestal, Z.J. Zhang, Nano Lett. 3 (2003) 1739.
[122] P. Tartaj, C.J. Serna, J. Am. Chem. Soc. 125 (2003) 15754.
[123] A.P. Philipse, M.P.B. van Bruggen, C. Pathmamanoharan, Langmuir 10 (1994) 92.
[124] D. Nagao, M. Yokoyama, N. Yamauchi, H. Matsumoto, Y. Kobayashi, M. Konno, Langmuir 24 (2008) 9804.
[125] D.Y. Ju, P. Bian, G.L. Qing, D. Lu, H. He, Key Eng. Mater. 368–372 (Part 2) (2008) 1366.
[126] A.-L. Morel, S.I. Nikitenko, K. Gionnet, A. Wattiaux, J. Lai-Kee-Him, C. Labrugere, B. Chevalier, G. Deleris, C. Petibois, A. Brisson, M. Simonoff, ACS Nano. 2 (2008) 847.
[127] H. Xu, L. Cui, N. Tong, H. Gu, J. Am. Chem. Soc. 128 (2006) 15582.
[128] Y. Zhu, H. Da, X. Yang, Y. Hu, Colloids Surf. A: Physicochem. Eng. Aspects 231 (2003) 123.
[129] Z. Liu, G. Yi, H. Zhang, J. Ding, Y. Zhang, J. Xue, Chem. Commun. (2008) 694.
[130] M. Stjerndahl, M. Andersson, H.E. Hall, D.M. Pajerowski, M.W. Meisel, R.S. Duran, Langmuir 24 (2008) 3532.
[131] R.P. Hodgkins, A. Ahniyaz, K. Parekh, L.M. Belova, L. Bergstrom, Langmuir 23 (2007) 8838.
[132] S.I. Stoeva, F. Huo, J.S. Lee, C.A. Mirkin, J. Am. Chem. Soc. 127 (2005) 15362.
[133] J. Ge, Y. Hu, M. Biasini, W.P. Beyermann, Y. Yin, Angew. Chem. Int. Ed. 46 (2007) 4342.
[134] T. Sen, A. Sebastianelli, I.J. Bruce, J. Am. Chem. Soc. 128 (2006) 7130.
[135] J. Kim, J.E. Lee, J. Lee, J.H. Yu, B.C. Kim, K. An, Y. Hwang, C.H. Shin, J.G. Park, J. Kim, T. Hyeon, J. Am. Chem. Soc. 128 (2006) 688.
[136] W. Zhao, J. Gu, L. Zhang, H. Chen, J. Shi, J. Am. Chem. Soc. 127 (2005) 8916.
[137] E.M. Claesson, A.P. Philipse, Langmuir 21 (2005) 9412.
[138] K.M. Kant, K. Sethupathi, M.S.R. Rao, J. Appl. Phys. 103 (2008) 1, 07D501/1.
[139] P. Tartaj, C.J. Serna, Chem. Mater. 14 (2002) 4396.
[140] P. Tartaj, T. Gonzalez-Carreno, C.J. Serna, J. Phys. Chem. B 107 (2003) 20.
[141] X. Ji, R. Shao, A.M. Elliott, R.J. Stafford, E. Esparza-Coss, J.A. Bankson, G. Liang, Z.-P. Luo, K. Park, J.T. Markert, C. Li, J. Phys. Chem. C 111 (2007) 6245.
[142] S. Lin, G. Yao, D. Qi, Y. Li, C. Deng, P. Yang, X. Zhang, Anal. Chem. 80 (2008) 3655.
[143] C.L. Chiang, C.S. Sung, C.Y. Chen, J. Magn. Magn. Mater. 305 (2006) 483.
[144] R. Abu-Reziq, H. Alper, D. Wang, M.L. Post, J. Am. Chem. Soc. 128 (2006) 5279.

[145] H.H. Yang, S.Q. Zhang, X.L. Chen, Z.X. Zhuang, J.G. Xu, X.R. Wang, Anal. Chem. 76 (2004) 1316.
[146] M. Fang, P.S. Grant, M.J. McShane, G.B. Sukhorukov, V.O. Golub, Y.M. Lvov, Langmuir 18 (2002) 6338.
[147] J. Ge, T. Huynh, Y. Hu, Y. Yin, Nano Lett. 8 (2008) 931.
[148] R. Abu-Reziq, D. Wang, M. Post, H. Alper, Chem. Mater. 20 (2008) 2544.
[149] S. Yitzhaki, E. Zahavy, C. Oron, M. Fisher, A. Keysary, Anal. Chem. 78 (2006) 6670.
[150] A.D. Ebner, J.A. Ritter, J.D. Navratil, Ind. Eng. Chem. Res. 40 (2001) 1615.
[151] Z. Zhang, L. Zhang, L. Chen, L. Chen, Q.H. Wan, Biotechnol. Prog. 22 (2006) 514.
[152] T.-J. Yoon, J.S. Kim, B.G. Kim, K.N. Yu, M.-H. Cho, J.-K. Lee, Angew. Chem. Int. Ed. 44 (2005) 1068.
[153] M. Liong, J. Lu, M. Kovochich, T. Xia, S.G. Ruehm, A.E. Nel, F. Tamanoi, J.I. Zink, ACS Nano. 2 (2008) 889.
[154] X.M. Qian, S.M. Nie, Chem. Soc. Rev. 37 (2008) 912.
[155] J. Pĭerez-Juste, I. Pastoriza-Santos, L.M. Liz-Marzĭan, P. Mulvaney, Coord. Chem. Rev. 249 (2005) 1870.
[156] S. Eustis, M.A. el-Sayed, Chem. Soc. Rev. 35 (2006) 209.
[157] H. Wang, D.W. Brandl, P. Nordlander, N.J. Halas, Acc. Chem. Res. 40 (2007) 53.
[158] E. Prodan, C. Radloff, N.J. Halas, P. Nordlander, Science 302 (2003) 419.
[159] S. Lal, S.E. Clare, N.J. Halas, Acc. Chem. Res. (2008).
[160] R.S. Elghanian, J.J.R.C. Mucic, R.L. Letsinger, C.A. Mirkin, Science 277 (1997) 1078.
[161] Y.C. Cao, R. Jin, C.A. Mirkin, Science 297 (2002) 1536.
[162] K. Aslan, M. Wu, J.R. Lakowicz, C.D. Geddes, J. Am. Chem. Soc. 129 (2007) 1524.
[163] S. Xu, S. Hartvickson, J.X. Zhao, Langmuir 24 (2008) 7492.
[164] Y. Lu, Y. Yin, Z. Li, Y. Xia, Nano Lett. 2 (2002) 785.
[165] Y. Han, J. Jiang, S.S. Lee, J.Y. Ying, Langmuir 24 (2008) 5842.
[166] C. Graf, D.L.J. Vossen, A. Imhof, A. van Blaaderen, Langmuir 19 (2003) 6693.
[167] L.M. Liz-Marzán, M. Giersig, P. Mulvaney, Langmuir 12 (1996) 4329.
[168] N.R. Jana, C. Earhart, J.Y. Ying, Chem. Mater. 19 (2007) 5074.
[169] A.T. Heitsch, D.K. Smith, R.N. Patel, D. Ress, B.A. Korgel, J. Solid State Chem. 181 (2008) 1590.
[170] S. Cavaliere-Jaricot, M. Darbandi, T. Nann, Chem. Commun. 20 (2007) 2031.
[171] M. Roca, A.J. Haes, J. Am. Chem. Soc. 130 (2008) 14273.
[172] Y. Shi, T. Asefa, Langmuir 23 (2007) 9455.
[173] J. Kim, W.W. Bryan, T.R. Lee, Langmuir 24 (2008) 11147.
[174] S.L. Westcott, S.J. Oldenburg, T.R. Lee, N.J. Halas, Langmuir 14 (1998) 5396.
[175] L. Zhang, Y. Feng, L. Wang, J. Zhang, M. Chen, D. Qian, Mater. Res. Bull. 42 (2007) 1457.
[176] B.E. Brinson, J.B. Lassiter, C.S. Levin, R. Bardhan, N. Mirin, N.J. Halas, Langmuir 24 (2008) 14166.
[177] Y. Sun, Y. Xia, Analyst 128 (2003) 686.
[178] C. Loo, A. Lowery, N.J. Halas, J. West, R. Drezek, Nano Lett. 5 (2005) 709.
[179] A.M. Gobin, M.H. Lee, N.J. Halas, W.D. James, R.A. Drezek, J.L. West, Nano Lett. 7 (2007) 1929.
[180] M. Choi, K.J. Stanton-Maxey, J.K. Stanley, C.S. Levin, R. Bardhan, D. Akin, S. Badve, J. Sturgis, J.P. Robinson, R. Bashir, N.J. Halas, S.E. Clare, Nano Lett. 7 (2007) 3759.
[181] O.G. Tovmachenko, C. Graf, D.J. van den Heuvel, A. van Blaaderen, H.C. Gerritsen, Adv. Mater. 18 (2006) 91.
[182] Y. Chen, K. Munechika, D.S. Ginger, Nano Lett. 7 (2007) 690.
[183] F. Tam, G.P. Goodrich, B.R. Johnson, N.J. Halas, Nano Lett. 7 (2007) 496.
[184] J. Zhang, Y. Fu, J.R. Lakowicz, J. Phys. Chem. C 111 (2007) 50.
[185] T. Zidki, H. Cohen, D. Meyerstein, D. Meisel, J. Phys. Chem. C 111 (2007) 10461.
[186] A.J. Sandee, J.N.H. Reek, P.C.J. Kamer, P.W.N.M. van Leeuwen, J. Am. Chem. Soc. 123 (2001) 8468.
[187] M.K. Richmond, S.L. Scott, H. Alper, J. Am. Chem. Soc. 123 (2001) 10521.
[188] B.D. Chandler, A.B. Schabel, L.H. Pignolet, J. Phys. Chem. B 105 (2001) 149.
[189] P. Barbaro, C. Bianchini, V. Dal Santo, A. Meli, S. Moneti, R. Psaro, A. Scaffidi, L. Sordelli, F. Vizza, J. Am. Chem. Soc. 128 (2006) 7065.
[190] C. Bianchini, D.G. Burnaby, J. Evans, P. Frediani, A. Meli, W. Oberhauser, R. Psaro, L. Sordelli, F. Vizza, J. Am. Chem. Soc. 121 (1999) 5961.
[191] T.J. Terry, T.D.P. Stack, J. Am. Chem. Soc. 130 (2008) 4945.
[192] R.M. Rioux, H. Song, J.D. Hoefelmeyer, P. Yang, G.A. Somorjai, J. Phys. Chem. B 109 (2005) 2192.
[193] Z. Konya, V.F. Puntes, I. Kiricsi, J. Zhu, J.W. Ager, M.K. Ko, H. Frei, P. Alivisatos, G.A. Somorjai, Chem. Mater. 15 (2003) 1242.
[195] G. Gupta, C.A. Stowell, M.N. Patel, X. Gao, M.J. Yacaman, B.A. Korgel, K.P. Johnston, Chem. Mater. 18 (2006) 6239.
[194] Y. Yang, S. Lim, G. Du, C. Wang, D. Ciuparu, Y. Chen, G.L. Haller, J. Phys. Chem. B 110 (2006) 5927.
[196] D. Panayotov, P. Kondratyuk, J.T. Yates, Langmuir 20 (2004) 3674.
[197] D.A. Panayotov, D.K. Paul, J.T. Yates, J. Phys. Chem. B 107 (2003) 10571.
[198] Y. Li, C.-Y. Wu, Environ. Sci. Technol. 40 (2006) 6444.
[199] N. Kamil, M.K. El Amrani, N. Benjelloun, Z. Naturforsch. B: J. Chem. Sci. 61 (2006) 1311.
[200] M. Hirano, K. Ota, H. Iwata, Chem. Mater. 16 (2004) 3725.
[201] J. Marugan, M.-J. Lopez-Munoz, R. van Grieken, J. Aguado, Ind. Eng. Chem. Res. 46 (2007) 7605.
[202] X. Jiang, T. Wang, J. Am. Chem. Soc. 91 (2008) 46.
[203] B. Bonelli, M. Cozzolino, R. Tesser, M. Di Serio, M. Piumetti, E. Garrone, E. Santacesaria, J. Catal. 246 (2007) 293.
[204] Y.Y. Pu, J.Z. Fang, F. Peng, H. Li, Chin. J. Inorg. Chem. 23 (2007) 1045.
[205] M.S. Lee, G.D. Lee, S.S. Park, C.S. Ju, K.T. Lim, S.S. Hong, Res. Chem. Intermediat. 31 (2005) 379.
[206] S.H. Kim, K.D. Kim, K.Y. Song, H.T. Kim, J. Ind. Eng. Chem. 10 (2004) 435.
[207] S.S. Hong, M.S. Lee, C.S. Ju, G.D. Lee, S.S. Park, K.T. Lim, Catal. Today 93–95 (2004) 871.
[208] J.L. de Souza, F. Fabri, R. Buffon, U. Schuchardt, Appl. Catal. A: Gen. 323 (2007) 234.
[209] H. Zhang, X. Luo, J. Xu, B. Xiang, D. Yu, J. Phys. Chem. B 108 (2004) 14866.
[210] A.A. Ismail, I.A. Ibrahim, M.S. Ahmed, R.M. Mohamed, H. El-Shall, J. Photochem. Photobiol. A: Chem. 163 (2004) 445.
[211] L.C. Chen, C.M. Huang, Ind. Eng. Chem. Res. 43 (2004) 6446.
[212] J.W. Lee, S. Kong, W.S. Kim, J. Kim, Mater. Chem. Phys. 106 (2007) 39.
[213] J. Yang, L. Zhu, J. Zhang, Y. Zhang, Y. Tang, React. Kinet. Catal. Lett. 91 (2007) 21.
[214] C. Shifu, C. Gengyu, Surf. Coat. Technol. 200 (2006) 3637.
[215] K. Guan, Surf. Coat. Technol. 191 (2005) 155.
[216] J. Marugan, M.J. Lopez-Munoz, R. vanGrieken, J. Aguado, Ind. Eng. Chem. Res. (2007).
[217] M. Gartner, V. Dremov, P. Muller, H. Kisch, ChemPhysChem 6 (2005) 714.
[218] T.-V. Nguyen, H.-C. Lee, M.A. Khan, O.B. Yang, Sol. Energy 81 (2007) 529.
[219] E. Palomares, J.N. Clifford, S.A. Haque, T. Lutz, J.R. Durrant, J. Am. Chem. Soc. 125 (2003) 475.
[220] T.L. Hsiung, H.P. Wang, H.C. Wang, Radiat. Phys. Chem. 75 (2006) 2042.
[221] M. Cozzolino, M. Di Serio, R. Tesser, E. Santacesaria, Appl. Catal. A: Gen. 325 (2007) 256.
[222] H.J. Kim, Y.G. Shul, H. Han, Top. Catal. 35 (2005) 287.
[223] Y.G. Shul, H.J. Kim, S.J. Haam, H.S. Han, Res. Chem. Intermediat. 29 (2003) 849.
[224] J. Wang, S. Uma, K.J. Klabunde, Appl. Catal. B: Environ. 48 (2004) 151.